Mon. Not. R. Astron. Soc. **000**, 1–19 (2014) Printed April 10, 2014 (MN LATEX style file v2.2)

Chemical evolution of classical and ultra-faint dwarf spheroidal galaxies

F. Vincenzo[1⋆], F. Matteucci[1,2,3⋆], S. Vattakunnel[1,2] and G. A. Lanfranchi[4]
[1] *Dipartimento di Fisica, Sezione di Astronomia, Università di Trieste, via G.B. Tiepolo 11, 34100, Trieste, Italy*
[2] *INAF Osservatorio Astronomico di Trieste, via G.B. Tiepolo 11, 34100, Trieste, Italy*
[3] *INFN, Sezione di Trieste, Via Valerio 2, 34100, Trieste, Italy*
[4] *Núcleo de Astrofísica Teórica, Universidade Cruzeiro do Sul - Rua Galvão Bueno 868, CEP 01506-000, São Paulo, Brazil*

arXiv:1404.2476v1 [astro-ph.GA] 9 Apr 2014

Accepted 2014 April 8. Received 2014 April 1; in original form 2014 February 11.

ABSTRACT

We present updated chemical evolution models of two dwarf spheroidal galaxies (Sculptor and Carina) and the first detailed chemical evolution models of two ultra-faint dwarfs (Hercules and Boötes I). Our results suggest that the dwarf spheroidals evolve with a low efficiency of star formation, confirming previous results, and the ultra-faint dwarfs with an even lower one. Under these assumptions, we can reproduce the stellar metallicity distribution function, the $[\alpha/Fe]$ vs. $[Fe/H]$ abundance patterns and the total stellar and gas masses observed at the present time in these objects. In particular, for the ultra-faint dwarfs we assume a strong initial burst of star formation, with the mass of the system being already in place at early times. On the other hand, for the classical dwarf spheroidals the agreement with the data is found by assuming the star formation histories suggested by the Color-Magnitude diagrams and a longer time-scale of formation via gas infall. We find that all these galaxies should experience galactic winds, starting in all cases before 1 Gyr from the beginning of their evolution. From comparison with Galaxy data, we conclude that it is unlikely that the ultra-faint dwarfs have been the building blocks of the whole Galactic halo, although more data are necessary before drawing firm conclusions.

Key words: stars: abundances - galaxies: abundances - galaxies: evolution - galaxies: formation - galaxies: dwarf - galaxies: Local Group - galaxies: individual (Sculptor, Carina, Hercules, Boötes I)

1 INTRODUCTION

Orbiting around the Milky Way, there is a large number of satellite galaxies, most of which have so low average surface brightnesses and small effective radii that their detection was very difficult in the past: from 1937 up to 1994, only nine of them were discovered and that number remained unchanged until 2005. They are the so-called *classical dwarf spheroidal galaxies* (dSphs), which are among the least luminous and most dark matter (DM) dominated galaxies which are observed today in the Universe. Dwarf spheroidal galaxies are classified as early-type since they are observed to possess very low gas mass at the present time and their stars are very iron-poor when compared to the Sun (see Tolstoy et al. 2009 and Koch 2009 for an exhaustive review).

Color-magnitude diagram (CMD) fitting analysis revealed star formation rate (SFR) in dSphs to have been either continuous for a long time or occurring in bursts. All dSph galaxies host an underlying very old stellar population with age $\gtrsim$ 10 Gyr (e.g. Grebel 1997), and some of them are dominated by an intermediate-age stellar population with age in the range $4-8$ Gyr (Dall'Ora et al. 2003). Very few dSphs have been observed to host younger stars, which populate the so-called "blue plume" in the CMD, sign of a relatively recent star formation activity, which occurred up to $\sim 2-3$ Gyr ago (Monelli et al. 2003).

All such features led cosmologists to hypothesize dSphs to be the evolved small progenitor systems which merged in the past to form the actual large structures in the Universe as the stellar halo of the Milky Way, in the framework of the ΛCDM standard cosmological model (Helmi & White 1999; Bullock et al. 2001; Harding et al. 2001; Bullock & Johnston 2005). However, successive deeper investigations revealed them not to possess all the right properties to be the aforementioned hypothetical survived

⋆ E-mail: vincenzo@oats.inaf.it; matteucc@oats.inaf.it

© 2014 RAS

progenitors of the Galactic halo (see Helmi et al. 2006 and Catelan 2009 and references therein).

The Sloan Digital Sky Survey (SDSS) allowed in the past few years (from 2005 up to the present time) to discover a large number of new dwarf galaxies orbiting around the Milky Way with physical properties very similar to dSph galaxies but average surface brightnesses and effective radii even much smaller (see, e.g., Belokurov et al. 2007, 2010): for such reasons, they have been named as *ultra-faint dwarf spheroidal galaxies* (UfDs). That is a mere naming convention, without any real physical motivation, since UfDs extend to fainter magnitudes and lower masses the same observed physical properties of dSphs. In fact UfD galaxies do not contain any gas at the present time and their stars are on average very iron-poor, with age $\gtrsim 10-12$ Gyr (Okamoto & Arimoto 2012; Brown et al. 2013). So UfDs do not show any recent star formation activity. Such stellar systems soon aroused great interest in the scientific community, either for their extreme observed characteristics, or because such characteristics might shed light on the conditions of the Universe in the first billion years of its evolution (see Belokurov 2013 for a detailed discussion). The UfD environment constitutes the best candidate for verifying whether a first population of very massive and extremely metal-poor stars (the so-called Population III) might have existed or not. Such stars, at their death, should have enriched the interstellar medium (ISM) with some metals and therefore they might have left a chemical signature in the stars which were born immediately after, as some of the UfD stars (Ferrara 2012). As Salvadori & Ferrara (2012) had envisaged, this hypothesis might be supported by the observation of carbon-enhanced metal-poor (CEMP) stars in some UfD galaxies (Norris et al. 2010; Gilmore et al. 2013), which might be directly linked to the CEMP-Damped Ly-α systems observed in the spectra of quasars at high redshift (Cooke et al. 2011a,b). In this scenario, the latter might be the high-redshift unevolved counterparts of some of the UfD galaxies.

Aim of this work is to study how dSph and UfD galaxies have evolved, by reconstructing - going back in time - the chemical enrichment history of their ISM, starting from the chemical abundances derived today in the atmospheres of their stars. We will adopt a detailed chemical evolution model which is able to follow the evolution of several chemical species (H, He, C, N, O, α-elements, Fe-peak elements, s- and r- process elements). This model is based on that presented by Lanfranchi & Matteucci (2004) and then used also in the works of Lanfranchi et al. (2006a), Lanfranchi et al. (2006b), Lanfranchi & Matteucci (2007), Lanfranchi et al. (2008), Cescutti et al. (2008), and Lanfranchi & Matteucci (2010).

Lanfranchi & Matteucci (2004) modeled the chemical evolution of six dSphs of the Local Group including Sextans, Sculptor, Sagittarius, Draco, Ursa Minor and Carina. Their main conclusions were that dSphs suffered from very low star formation efficiency, which caused the iron pollution from Type Ia SNe to become important when the $[Fe/H]$ of galaxy ISM was still very low. In this manner, and by assuming also intense galactic winds, they were able to explain the observed decrease in the trends of $[\alpha/Fe]$ vs. $[Fe/H]$. Galactic winds prevent the galaxy to form stars soon after the onset of the outflow and this leads the stellar metallicity distribution function (MDF) in dSphs to be peaked towards low $[Fe/H]$ abundances, almost 1.5 dex below the one of Milky Way disc in the solar neighborhood, in agreement with observations.

As interesting papers appeared recently, Romano & Starkenburg (2013) modeled the chemical evolution of Sculptor by means of a new approach in a full cosmological framework, whereas Koch et al. (2012, 2013) present a first chemical evolution model of the Hercules UfD, based on the same numerical code we use in this work.

Here we focus on the chemical evolution of Sculptor and Carina, for which newer data are available, but especially we model the evolution of UfDs: Hercules and Boötes I. In Section 2 we describe the adopted chemical evolution model. In Section 3 the data sample is presented and in Section 4 the results are shown. Finally, in Section 5 some conclusions are drawn.

2 DESCRIPTION OF THE MODEL

2.1 Assumptions

We assumed dSph and UfD galaxies to form by infall of primordial gas in a pre-existing DM halo. The infall rate obeys to a decaying exponential law with very short typical timescales and the so-called *infall mass* represents the reservoir of the infalling gas from which the stars form.

Thanks to the detailed treatment of the main physical processes involved in the chemical enrichment of the galaxy ISM, we were able to predict the trends of the chemical abundances of many elements relative to iron as a function of $[Fe/H]$[1], the MDF and the total stellar and gas masses at the present time. Other observational constraints are represented by the history of star formation (SFH), which may be characterized either by a single long episode or by several bursts of star formation, according to the CMD-fitting analysis; the total mass of the DM halo and, finally, the effective radius of the luminous baryonic component of the galaxy. We assumed, when we do not have any information, a diffuse dark matter halo for these galaxies, with $S = \frac{r_L}{r_{DM}}$ between 0.2 and 0.4, where r_{DM} represents the core radius of each galaxy DM halo.

The main assumptions of the model, which is similar to that of Lanfranchi & Matteucci (2004), are the following:

(i) each galaxy is modelled as a one zone with instantaneous and complete mixing of gas within it;
(ii) stellar lifetimes are taken into account (no instantaneous recycling approximation);
(iii) nucleosynthesis prescriptions include the yields of Iwamoto et al. (1999) for Type Ia SNe, the yields of Woosley & Weaver (1995) (with the corrections suggested by François et al. 2004) for massive stars, and the metallicity-dependent yields of van den Hoek & Groenewegen (1997) for low and intermediate mass stars.

[1] We will use the following notation for the stellar chemical abundances: $[X/Y] = \log_{10}(N_X/N_Y)_\star - \log_{10}(N_X/N_Y)_\odot$, where N_X and N_Y are the volume density number of the atoms of the species X and Y respectively.

The galaxy can lose gas through galactic winds, which develop when the thermal energy of the gas $E_g^{th}(t)$ equals the binding energy of the gas $E_g^b(t)$. The latter quantity $E_g^b(t)$ is calculated by means of assumptions concerning the presence and the distribution of the DM which, for dSphs and UfDs, is usually represented as a diffuse halo (see Bradamante et al. 1998), whereas the thermal energy of gas $E_g^{th}(t)$ is primarily determined by the energy deposited by SN explosions into the ISM (see also for more details Yin et al. 2011 and references therein).

2.2 Basic equations

If $M_{g,i}(t)$ is the gas mass in the form of an element i at the time t within the ISM, its temporal evolution is described by the following basic equation:

$$\dot{M}_{g,i} = -\psi(t)X_i(t) + R_i(t) + (\dot{M}_{g,i})_{inf} - (\dot{M}_{g,i})_{out}, \quad (1)$$

where the quantity $X_i(t) = M_{g,i}(t)/M_{gas}(t)$ represents the abundance by mass of the element i, with the summation over the abundances of all the elements in the gas mixture being equal to unity, and $M_{gas}(t)$ is the total gas mass of the galaxy at the time t. The functions $\phi(m)$ and $\psi(t)$ represent the initial mass function (IMF) and the star formation rate (SFR), respectively.

(i) The first term in the right hand side of Eq.(1) represents the rate at which chemical elements are subtracted from the ISM by star formation activity. The SFR has the following simple form (Schmidt law with $k = 1$, Schmidt 1959):

$$\psi(t) = \frac{dM_{gas}}{dt} = \nu M_{gas}^k, \quad (2)$$

where ν is the star formation efficiency ($[\nu] = Gyr^{-1}$), which represents the intensity of the star formation rate and we assume in this work $k = 1$. The inverse of ν corresponds to the typical time-scale for the complete gas consumption if star formation were the only physical process affecting the ISM.
(ii) The second term in Eq.(1), $R_i(t)$, represents the returned mass in the form of an element i that stars eject into the ISM per unit time through stellar winds and supernova explosions. This term contains all the prescriptions concerning stellar yields and supernova progenitor models.
(iii) The third term in Eq.(1), $(\dot{M}_{g,i})_{inf}$, is the rate at which the element i is accreted during the initial infall event. The rate of gas infall is defined as:

$$(\dot{M}_{g,i})_{inf} = A \cdot X_{i,inf} \cdot e^{-t/\tau}, \quad (3)$$

where A is a suitable constant such that

$$\sum_i \int_0^{t_G} dt\ A \cdot X_{i,inf} \cdot e^{-t/\tau} = M_{inf}, \quad (4)$$

with M_{inf} being the infall mass and τ the so-called infall time-scale of the mass accretion. The gas out of which dSph and UfD galaxies form is assumed to be of primordial chemical composition, namely $X_{i,inf} = 0$ for heavy elements. We assumed for dSphs an infall time-scale $\tau_{dSph} = 0.5$ Gyr, while for UfDs we adopted $\tau_{UfD} = 0.005$ Gyr, which is almost equivalent to assume the gas to be all present in the DM halo since the beginning. The reason for these choices will be clearer in the next sections and are dictated by fitting the observational constraints.

(iv) The last term in Eq.(1) represents the rate at which the element i is lost through galactic winds. For each element i, the rate of gas loss at the time t is assumed to be directly proportional to the SFR at the time t:

$$(\dot{M}_{g,i})_{out} = \omega_i \psi(t), \quad (5)$$

where ω_i are free parameters describing the efficiency of the galactic wind, i.e. the intensity of the rate of gas loss in the form of the element i. Here is all the information regarding the energy released by SNe, as well the efficiency with which that energy is transformed into gas escape velocity. For dSph and UfD galaxies we supposed the galactic wind to be *normal*, namely with the ω parameter being equal for all the chemical elements, although we tested also models with different kind of *differential* winds, following Marconi et al. (1994) and Recchi et al. (2001).

3 DATA SAMPLE

In general, we have selected - when possible - only high-resolution data and we have scaled all of them to the same Solar abundances (Asplund et al. 2009). The reason for this was to homogeneize the data as much as possible.

3.0.1 Sculptor dSph

Sculptor is a relatively faint ($M_V \approx -11.1$, from Mateo 1998) stellar system, located at a distance of 79 ± 4 kpc (Koch 2009) away from us. Its features make it a fair representative of a typical dSph galaxy of the Local Group and it is also one of the most extensively investigated. It hosts the most iron-poor stars ever observed in a dSph, with $[Fe/H] = -3.96 \pm 0.06$ dex (Tafelmeyer et al. 2010).

We used the dataset of chemical abundances presented by Shetrone et al. (2003), Tafelmeyer et al. (2010), Frebel et al. (2010) and Kirby & Cohen (2012). The data sample we used for the MDF is taken from Romano & Starkenburg (2013), who combined the data samples of the DART project (Battaglia et al. 2008a; Starkenburg et al. 2010) and of Kirby et al. (2009, 2010).

3.0.2 Carina dSph

Carina is located at a distance of 94 ± 5 kpc and belongs to the faintest dSphs of the Local Group ($M_V \approx -9.3$, $\mu_V = 25.5 \pm 0.4$ mag arcsec^{-2}, from Mateo 1998). In the dSph realm, Carina is almost unique, since its CMD reveals a bursty SFH, which gave rise to the today observed multiple stellar populations (Hurley-Keller et al. 1998; Tolstoy et al. 2003).

The dataset of chemical abundances we used for the comparisons with the predictions of our models have been taken from the following works: Shetrone et al. (2003), Koch et al. (2008a), Lemasle et al. (2012) and Venn et al. (2012). The observed MDF has been taken from Koch et al. (2006).

3.0.3 Hercules UfD

The Hercules UfD was discovered by Belokurov et al. (2007) from the analysis of Sloan Digital Sky Survey (SDSS) data.

The line of sight toward Hercules is heavily contaminated by Galactic foreground stars since it resides at a lower Galactic latitude than the other UfDs (de Jong et al. 2008). Furthermore, the mean radial velocity of Hercules stars is very similar to the mean radial velocity of thick disk stars.

Hercules appears clearly highly elongated, without any evidence of internal rotation ($\sigma_v \sim 3.72$ km s^{-1}, from Adén et al. 2009b). Such a large ellipticity with no rotational support might imply that Hercules is not in dynamical equilibrium and it is undergoing strong tidal distortions. Hercules lies at a distance of 132 ± 12 kpc from us, it has an absolute V-band magnitude $M_V = -6.6 \pm 0.3$ and a V-band surface brightness of only $\mu_V = 27.2 \pm 0.6$ mag arcsec^{-2} (see Adén et al. 2009b and references therein).

The data sample we used for the chemical abundances in the Hercules UfD is taken from Adén et al. (2011), which provide the chemical abundances of calcium and iron, the only elements actually available for this galaxy.

3.0.4 Boötes I UfD

The Boötes I UfD was discovered by Belokurov et al. (2006), from the analysis of SDSS data. Siegel (2006) estimated the distance of Boötes I by using 15 RR Lyrae variable stars as standard candles; they found a distance: $D = 62 \pm 4$ kpc, very similar to that of the outermost halo globular clusters in our Galaxy. Finally, Belokurov et al. (2006) reported an absolute magnitude $M_V = -5.8$ and an half-light radius $r_h \sim 220$ pc.

The data samples of chemical abundances have been taken from the works of Norris et al. (2010) and Gilmore et al. (2013) ("NY" analysis, from Norris et al. 2010). The observed MDF has been worked out by Lai et al. (2011), by expanding their own sample to include non-overlapping stars from Norris et al. (2010) and Feltzing et al. (2009). The data sample of Ishigaki et al. (2014), not considered in this work for its lower resolution than the other studies, shares three stars in common with Gilmore et al. (2013); in any case, the two data samples turn out to agree with each other in the final chemical abundances of the α-elements.

4 RESULTS

4.1 Chemical evolution of the Sculptor dSph

We assumed the galaxy to form from the accretion of $1.0 \cdot 10^8$ $M_\odot$ primordial gas, at an infall rate with a time-scale of 0.5 Gyr. According to what has been inferred observationally by means of the CMD-fitting analysis (de Boer et al. 2012), the SFH has been assumed to consist of only one long episode of star formation lasting 7 Gyr. Following the observations, the galaxy is characterized by a massive and extended dark matter halo, with a mass of $3.4 \cdot 10^8$ $M_\odot$ (Battaglia et al. 2008b) and we assumed a core radius $r_{DM} = 1$ kpc. The effective radius of the *luminous* (baryonic) component of the galaxy has been set at the value of 260 pc (Walker et al. 2009). So the ratio between the core radius of the dark matter halo and the effective radius of the *luminous* matter is $S = \frac{r_L}{r_{DM}} = 0.260$. We need these quantities in order to compute the binding energy of the gas

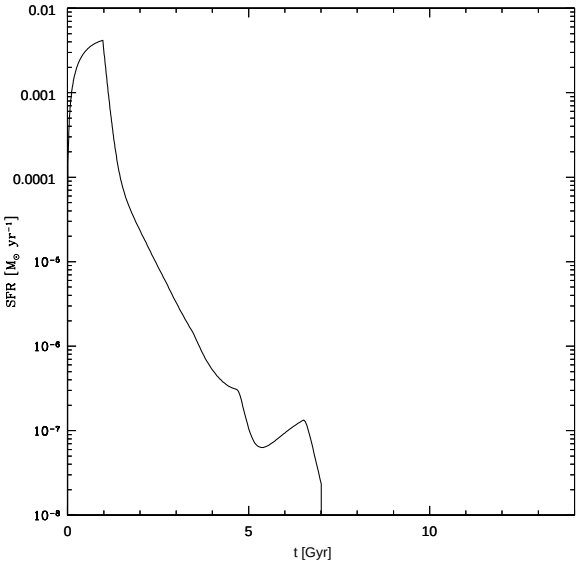

Figure 1. In this Figure we show the Sculptor SFR (in $M_\odot/yr$) as predicted by our model with $\nu = 0.05$ Gyr^{-1} and $\omega = 10$, which turned out to well reproduce at the same time the observed abundance ratio patterns and the MDF, as well as the other observed properties of the Sculptor dSph.

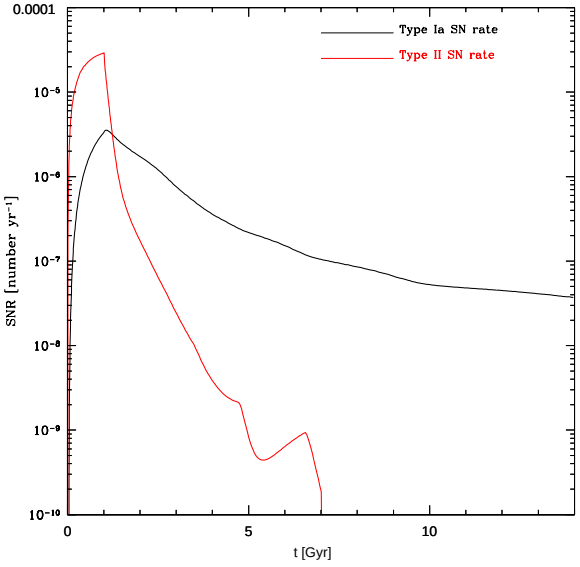

Figure 2. In this Figure we plot the Sculptor Type II and Type Ia supernova rates predicted by the same model as Fig.(1).

and so the time at which the galaxy developed the galactic wind. The complete set of the parameters characterizing the chemical evolution models performed for the Sculptor dSph is summarized in Table 1. We changed the values of ν (efficiency of star formation) and ω (wind parameter), in order to find a model able to reproduce the observed properties of the galaxy, such as the abundance ratios, the MDF and the present time gas and stellar masses. We tried models with $\omega = 5, 10, 15$ and 20; then, for each value of ω, we varied the

Sculptor: model parameters								
ν	ω	τ_{inf}	SFH	M_{inf}	M_{DM}	r_L	$S=\frac{r_L}{r_{DM}}$	IMF
$[Gyr^{-1}]$		[Gyr]	[Gyr]	$M_\odot$	$M_\odot$	$[pc]$		
0.01/0.05/0.1/0.2	5/10/15/20	0.5	$0-7$	$1.0\cdot10^8$	$3.4\cdot10^8$	260	0.260	Salpeter (1955)

Table 1. *Table:* we summarize here the specific characteristics of all the chemical evolution models performed for the Sculptor dSph. *Columns:* (1) star formation efficiency; (2) wind parameter; (3) infall time-scale; (4) period of major star formation activity (de Boer et al. 2012); (5) total infall gas mass; (6) mass of the dark matter halo (Battaglia et al. 2008b); (7) effective radius of the *luminous* (baryonic) matter (Walker et al. 2009); (8) ratio between the core radius of the dark matter halo and the effective radius of the *luminous* matter; (9) initial mass function.

Sculptor chemical evolution models					
Input parameters		Model predictions			
	ν	$M_{\star,fin}$	$M_{gas,fin}$	t_{wind}	$[Fe/H]_{peak}$
	$[Gyr^{-1}]$	$M_\odot$	$M_\odot$	[Gyr]	dex
$\omega=5$	0.01	$0.13\cdot10^7$	$0.26\cdot10^3$	2.48	-1.91
	0.05	$0.21\cdot10^7$	$0.12\cdot10^4$	1.01	-1.73
	0.1	$0.27\cdot10^7$	$0.19\cdot10^4$	0.66	-1.62
	0.2	$0.34\cdot10^7$	$0.15\cdot10^4$	0.38	-1.42
$\omega=10$	0.01	$0.12\cdot10^7$	$0.14\cdot10^3$	2.48	-1.93
	0.05	$0.18\cdot10^7$	$0.67\cdot10^3$	1.01	-1.79
	0.1	$0.21\cdot10^7$	$0.69\cdot10^3$	0.66	-1.71
	0.2	$0.24\cdot10^7$	$0.29\cdot10^3$	0.38	-1.60
$\omega=15$	0.01	$0.12\cdot10^7$	$0.97\cdot10^2$	2.48	-1.94
	0.05	$0.17\cdot10^7$	$0.46\cdot10^3$	1.01	-1.81
	0.1	$0.19\cdot10^7$	$0.30\cdot10^3$	0.66	-1.74
	0.2	$0.20\cdot10^7$	$0.11\cdot10^3$	0.38	-1.67
$\omega=20$	0.01	$0.12\cdot10^7$	$0.75\cdot10^2$	2.48	-1.94
	0.05	$0.17\cdot10^7$	$0.35\cdot10^3$	1.01	-1.81
	0.1	$0.17\cdot10^7$	$0.12\cdot10^3$	0.66	-1.76
	0.2	$0.18\cdot10^7$	$0.58\cdot10^2$	0.38	-1.71

Table 2. *Table:* we reported for each model its main predictions. *Columns:* (1) wind parameter; (2) star formation efficiency; (3) predicted actual total stellar mass; (4) predicted actual total gas mass; (5) time of the onset of the galactic wind; (6) peak of the stellar MDF predicted by the models.

star formation efficiency ν, setting it at the following values: $\nu=0.01, 0.05, 0.1$, and $0.2\ Gyr^{-1}$.

In Fig.(1) we show the trend of the predicted SFR as a function of time. By looking at this Figure, in the earliest stages of the galaxy evolution, the SFR increases very steeply because of the large amount of pristine gas accreted during the infall in a very short time-scale. In fact, we have assumed the SFR, $\psi(t)$, to be proportional to the gas mass (see Eq.(2)). After the majority of the reservoir of gas M_{inf} has been accreted, the star formation begins to decrease in time, since both SF activity and galactic wind subtract gas from the galaxy ISM.

In Fig.(2) we compare the predicted Type II and Type Ia supernova rates. While SNe Ia occur on a large range of time-scales (from ~ 35 Myr up to the age of the Universe), depending on the features of the progenitor system, the Type II SN rate traces very closely the trend of the SFR, because of the very short typical time-scales involved (from ~ 1 up to ~ 35 Myr). Thus, after the infall is substantially reduced, the Type II SN rate decreases much more steeply than the Type Ia SN rate. We predict a present time SNIa rate of $6.66\cdot10^{-4}\ SNuM$, where $SNuM$ represents the rate with units of one SN per 100 yr per $10^{10}\ M_\odot$ stellar mass (Li et al. 2011).

For each of the models we have calculated, Tab.(2) reports its main predictions regarding the stellar and gas masses at the present time, the time of onset of the galactic wind, and the $[Fe/H]$-peak of the stellar MDF. In the first two columns, Tab.(2) shows again the input parameters (ν and ω) characterizing each model.

By looking at Tab.(2), for a fixed value of the wind parameter ω, models with increasing star formation efficiencies predict slightly larger final total stellar masses and, at the same time, slightly lower final total gas masses. This happens both because star formation is more efficient, and because the galactic wind is predicted to start earlier and earlier, being larger the number of SN events triggering the wind.

The wind parameter ω - which roughly represents the efficiency with which the chemical elements are carried out of

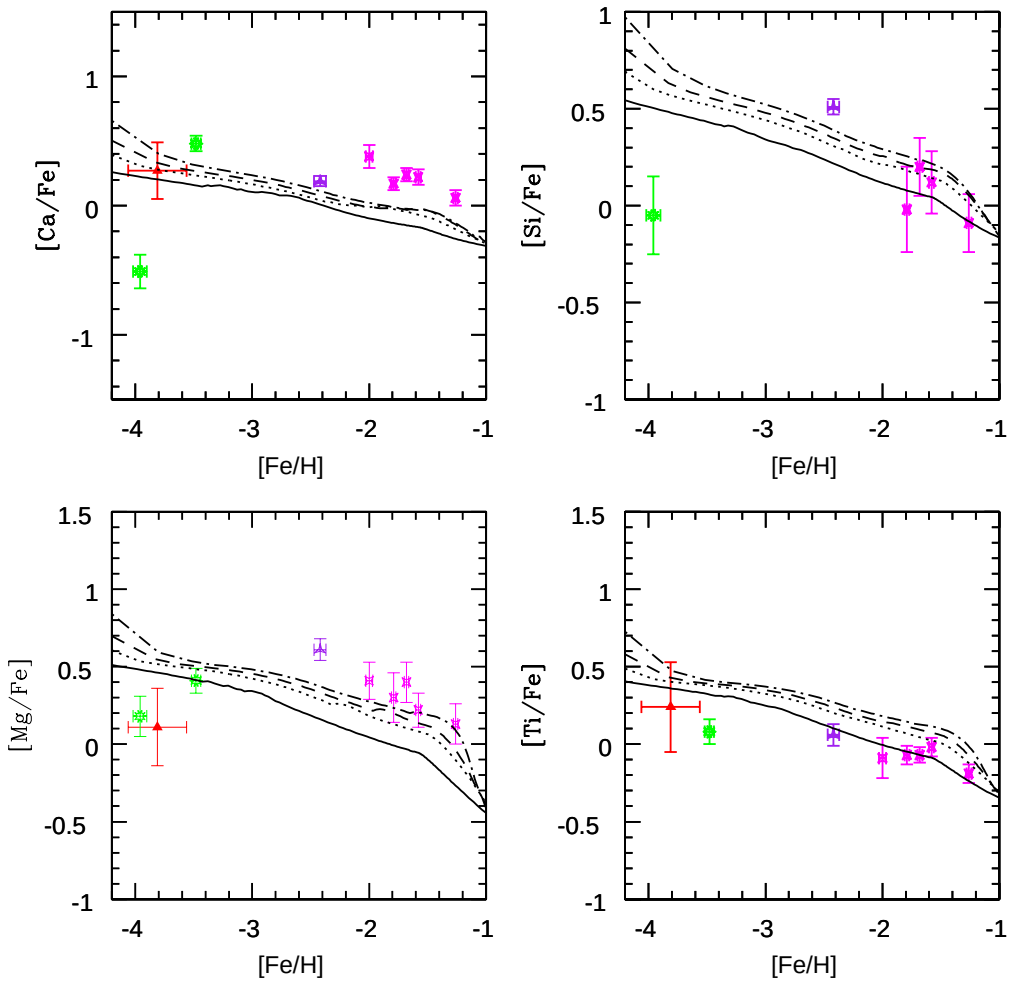

Figure 3. In this Figure, we compare the observed Sculptor $[\alpha/Fe]$ vs. $[Fe/H]$ abundance patterns for calcium, silicon, titanium and magnesium with the trends predicted by our $\omega = 10$ models. Data are from Shetrone et al. (2003, in magenta), Tafelmeyer et al. (2010, in green), Frebel et al. (2010, in red) and Kirby & Cohen (2012, in purple). The solid line corresponds to the model with $\nu = 0.01\ Gyr^{-1}$, the dotted line to the model with $\nu = 0.05\ Gyr^{-1}$, the long dashed line to the model with $\nu = 0.1\ Gyr^{-1}$ and the dot-dashed line to the model with $\nu = 0.2\ Gyr^{-1}$. Low star formation efficiencies ν cause to be small the amount of iron coming from Type II SNe. So, when Type Ia SNe start to pollute the ISM with large amounts of iron, the $[Fe/H]$ of the ISM is very low. This gives rise to the decrease of $[\alpha/Fe]$ as $[Fe/H]$ increases. Furthermore, the onset of the galactic wind causes a steepening in the decrease of $[\alpha/Fe]$ as a function of $[Fe/H]$

the galaxy - characterizes the intensity of the outflow rate. By increasing the wind parameter ω, our models predict the final total gas mass to be lower, since the galactic wind removes the interstellar gas from the galaxy potential well more efficiently. Moreover, as one would expect, the final total stellar mass slightly decreases if the efficiency of the galactic wind is strengthened.

All the models at Tab.(2) predict final stellar masses which are of the same order of magnitude as the observed one $M_{\star,obs} = (1.2 \pm 0.6) \cdot 10^6\ M_\odot$, which has been derived by de Boer et al. (2012) by integrating the SFR up to the present time; however, this mass is still quite uncertain, since it strongly depends not only on the IMF adopted, but also on the overall CMD-fitting technique. Moreover, all the models predict very low final gas masses ($\sim 10^2 - 10^3\ M_\odot$), which are lower than $M_{HI} \approx 1.0 \cdot 10^4\ M_\odot$ estimated by Mateo (1998) and very much lower than the most recent estimate of Grcevich & Putman (2009), which inferred for Sculptor an upper limit in the HI mass of $M_{HI} < 2.34 \cdot 10^5\ M_\odot$, although affected by a very large uncertainty.

Finally, from Tab.(2), it is possible to appreciate the net effect of changing the star formation efficiency ν and the wind parameter ω on the MDF-peak. The lowest $[Fe/H]$ at which the MDF has its peak is obtained by the models with the lowest ν and the highest ω.

4.1.1 *Sculptor dSph: abundance ratios and interpretation*

As already mentioned, the α-elements are mainly produced by Type II SNe, on short time-scales, whereas the bulk of iron and iron-peak elements ($\sim 2/3$ of the total) are pro-

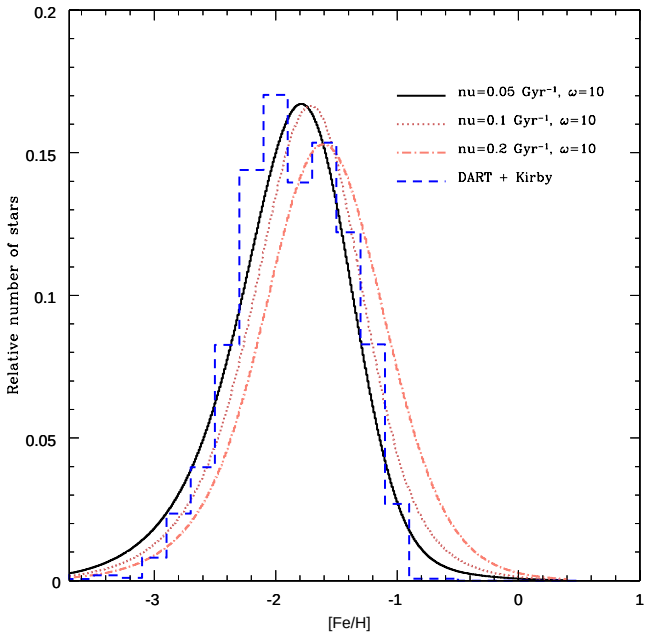

Figure 4. The Figure shows the comparison between the observed stellar MDF of the Sculptor dSph and the predictions of our $\omega = 10$ models. The observed dataset comes from Romano & Starkenburg (2013), who combined the data samples of the DART project (Battaglia et al. 2008a; Starkenburg et al. 2010) and of Kirby et al. (2009, 2010). By enhancing the star formation efficiency, the peak of the MDF shift towards higher $[Fe/H]$ abundance ratios, because of the shorter time-scales involved in the chemical enrichment of the ISM. At the same time, the height of the peak diminishes, because of the stronger outflow rates ($\propto \psi(t)$), which clean up the galaxy of the gas; that is more evident by passing from $\nu = 0.1\ Gyr^{-1}$ up to $\nu = 0.2\ Gyr^{-1}$. The best agreement is obtained with the $\nu = 0.05$ Gyr^{-1} and $\omega = 10$ model.

duced by Type Ia SNe on a very large range of typical time-scales. The residual quantities of iron and iron-peak elements ($\sim 1/3$ of the total) are synthesized by Type II SNe.

Different typical star formation time-scales can affect the $[\alpha/Fe]$ vs. $[Fe/H]$ diagram with a typical signature (Matteucci & Brocato 1990; Matteucci & Recchi 2001). In fact, low star formation efficiencies cause the amount of iron from Type II SNe to grow very slowly within the ISM. As the first Type Ia SNe start to explode, they deposit a large quantity of iron into the ISM and the $[\alpha/Fe]$ ratio is expected to steeply decrease at still very low $[Fe/H]$. Conversely, high star formation efficiencies give rise to large fractions of iron produced by Type II SNe. In this case, a plateau in the $[\alpha/Fe]$ vs. $[Fe/H]$ diagram is predicted and the decrease occurs at relatively high $[Fe/H]$ abundances (see Matteucci 2001). Therefore, the abundance ratios in dSph reflect their low SFR (Lanfranchi & Matteucci 2004). In Fig.(3) we show the effect of different ν values on the predicted $[\alpha/Fe]$ vs. $[Fe/H]$ relations. To lower further the SFR and thus steepening even more the decrease in the $[\alpha/Fe]$ vs. $[Fe/H]$, one can adopt higher values of the wind parameter ω. In fact, the galactic wind subtracts gas to the SF and makes it to decrease. In the models of Fig.(3), we assumed the outflow to remove all the chemical elements with the same efficiency, i.e. with same ω parameter.

We note that in Fig.(3) the data relative to Mg lie below our model predictions. The reason for this can be uncertainties in the data or more likely uncertainties in the Mg yields. These anomalous low-Mg stars have been often associated with inhomogeneous enrichment on small scales from, e.g., single or at least few SNe (Koch et al. 2008a,b; Simon et al. 2010; Frebel & Bromm 2012; Keller et al. 2014). However, in small systems we should expect that different regions of the ISM mix on small typical timescales and, if the star formation timescales are large enough (and this is the case for dSphs and UfDs), the ISM should have had enough time to mix before new star formation occurs. So we should expect that the enrichment in low-mass and small-scale systems, with very low star formation efficiencies, is more homogeneous rather than more inhomogeneous. In fact, the cooling time for these small systems could be quite low (see Recchi et al. 2002). Furthermore, dSphs seem to be supported by the random motions of stars rather than by regular motions. So, we expect that the thermalisation processes have been efficient and that the one-zone assumption is reasonable. Finally, small systems do not show evident abundance gradients and this is another indicator of a well mixed ISM.

4.1.2 Sculptor dSph: MDF and interpretation

One other important constraint to verify the goodness of a chemical evolution model is to check whether it is able to reproduce the observed stellar MDF. In Fig.(4), we show the comparison between the observed stellar MDF and our $\omega = 10$ models. As shown in this Figure, by increasing the star formation efficiency, the predicted stellar MDF peaks towards higher $[Fe/H]$ abundances, since shorter time-scales are involved in the galactic chemical enrichment produced by successive generations of stars. At the same time, by increasing the ν parameter (especially from $\nu = 0.1\ Gyr^{-1}$ to $\nu = 0.2\ Gyr^{-1}$), the height of the MDF peak diminishes because of the stronger outflow rate ($\propto \psi(t)$) which leaves, on average, less gas available for star formation. The model which best reproduces the MDF shape of Sculptor is characterized by a star formation efficiency $\nu = 0.05\ Gyr^{-1}$.

4.1.3 Sculptor dSph: previous models

One of the first detailed chemical evolution models of Sculptor was presented by Lanfranchi & Matteucci (2004). In this work we have adopted the same theoretical prescriptions and the same numerical code used in that first work

Lanfranchi & Matteucci (2004) did not possess yet an observed MDF dataset for the comparison with the models since only recently there have been obtained very precise determinations of the Sculptor SFH and physical characteristics, which have been used in our models as observational constraints.

However, although Lanfranchi & Matteucci (2004) had to work with very poorer dataset of chemical abundances, their predictions were similar to the results of this work. The main differences between the models calculated by this work and the ones of Lanfranchi & Matteucci (2004) are the following ones:

Carina: model parameters								
ν	ω	τ_{inf}	SFH	M_{inf}	M_{DM}	r_L	$S = \frac{r_L}{r_{DM}}$	IMF
$[Gyr^{-1}]$		[Gyr]	[Gyr]	$M_\odot$	$M_\odot$	$[pc]$		
0.05/0.1/0.2	5/10/20	0.5	$0-2\,;\,2-4\,;\,7-9\,;\,9-11$	$1.0\cdot10^8$	$4.0\cdot10^7$	290	0.3625	Salpeter (1955)

Table 3. *Table:* we summarize here the specific characteristics of all the chemical evolution models performed for the Carina dSph. *Columns:* (1) star formation efficiency; (2) wind parameter; (3) infall time-scale; (4) period of major star formation activity (Rizzi et al. 2003); (5) total infall gas mass; (6) mass of the dark matter halo (Gilmore et al. 2007); (7) effective radius of the *luminous* (baryonic) matter (Gilmore et al. 2007); (8) ratio between the core radius of the dark matter halo (Gilmore et al. 2007) and the effective radius of the *luminous* matter; (9) initial mass function.

Carina chemical evolution models					
Input parameters	Model predictions				
	ν	$M_{\star,fin}$	$M_{gas,fin}$	t_{wind}	$[Fe/H]_{peak}$
	$[Gyr^{-1}]$	$M_\odot$	$M_\odot$	[Gyr]	dex
$\omega = 5$	0.05	$0.16\cdot10^7$	$0.12\cdot10^4$	0.77	−1.87
	0.1	$0.20\cdot10^7$	$0.96\cdot10^3$	0.45	−1.71
	0.2	$0.28\cdot10^7$	$0.12\cdot10^4$	0.24	−1.50
$\omega = 10$	0.05	$0.13\cdot10^7$	$0.65\cdot10^3$	0.77	−1.90
	0.1	$0.14\cdot10^7$	$0.18\cdot10^3$	0.45	−1.88
	0.2	$0.17\cdot10^7$	$0.24\cdot10^3$	0.24	−1.55
$\omega = 20$	0.05	$0.12\cdot10^7$	$0.31\cdot10^3$	0.77	−1.91
	0.1	$0.11\cdot10^7$	$0.30\cdot10^2$	0.45	−1.90
	0.2	$0.11\cdot10^7$	$0.51\cdot10^2$	0.24	−1.87

Table 4. *Table:* we reported for each model its main predictions. *Columns:* (1) wind parameter; (2) star formation efficiency; (3) predicted actual total stellar mass; (4) predicted actual total gas mass; (5) time of the onset of the galactic wind; (6) peak of the stellar MDF predicted by the models.

(i) The galactic wind in Lanfranchi & Matteucci (2004) is *differential*, i.e. some elements - in particular the products of SNe Ia - are lost more efficiently than others from the galaxy, following Recchi et al. (2001).
(ii) The models of Lanfranchi & Matteucci (2004) assume a more extended and massive dark matter halo ($M_{DM} = 5.0\cdot10^9\ M_\odot$ and $S = \frac{r_L}{r_{DM}} = 0.1$) than our models.
(iii) The infall gas mass in Lanfranchi & Matteucci (2004) is slightly higher than ours. In fact it is: $M_{inf} = 5.0\cdot10^8\ M_\odot$.

Lanfranchi & Matteucci (2004) suggested as best model for Sculptor the one with $\nu = 0.2\ Gyr^{-1}$ and $\omega_i = 13$.

4.2 Chemical evolution of the Carina dSph

The most important difference between Sculptor and Carina resides in their SFH. While the Sculptor SFH is characterized by only one episode, with the SFR continuous for 7 Gyr, the Carina dSph has been observed, from the analysis of its CMD, to have undergone a bursty SFH. So, following Rizzi et al. (2003) and the suggestions of Lanfranchi et al. (2006b), we adopted for the Carina dSph a SFH characterized by 4 episodes, all lasting 2 Gyr, with the first two occurring from 0 to 4 Gyr and the second two occurring from 7 to 11 Gyr.

The galaxy DM halo is characterized by a total mass $M_{DM} = 4.0\cdot10^7\ M_\odot$, and a core radius $r_{DM} = 0.8\ kpc$ (Gilmore et al. 2007). The effective radius of the *luminous* (baryonic) matter has been set at the value $r_L = 290\ pc$ (Gilmore et al. 2007). So, the ratio between the core radius of the DM halo and the effective radius of the baryonic matter is $S = \frac{r_C}{r_L} = 0.3625$.

According to our model of chemical evolution, the galaxy assembled from the accretion of an *infall mass* $M_{inf} = 1.0\cdot10^8\ M_\odot$, made up of primordial gas, with the infall time-scale being assumed to be 0.5 Gyr.

In Tab.(3), we have summarized all the chemical evolution models we have computed for the Carina dSph. Following the procedure used for the Sculptor dSph, we varied again only the ν and the ω parameters, namely the star formation efficiency and the wind parameter, respectively.

In Fig.(5), it is shown the SFR of Carina dSph. By looking at that Figure, we can see that there is almost a continuous transition between the first ($0-2$ Gyr) and the second burst ($2-4$ Gyr), as well as from the third ($7-9$ Gyr) and the fourth burst ($9-11$ Gyr). This is due to the fact that the time interval between those episodes is so short that nor the galactic wind neither the gas restored by dying stars might have highly affected the gas mass and therefore the intensity of the SFR. In fact, the SFR has been assumed to be proportional to the gas mass in the galaxy. The discontinuity is clear only between the second ($2-4$ Gyr) and the third ($7-9$ Gyr) burst: during the temporary break ($4-7$ Gyr) of star formation, the gas mass in the

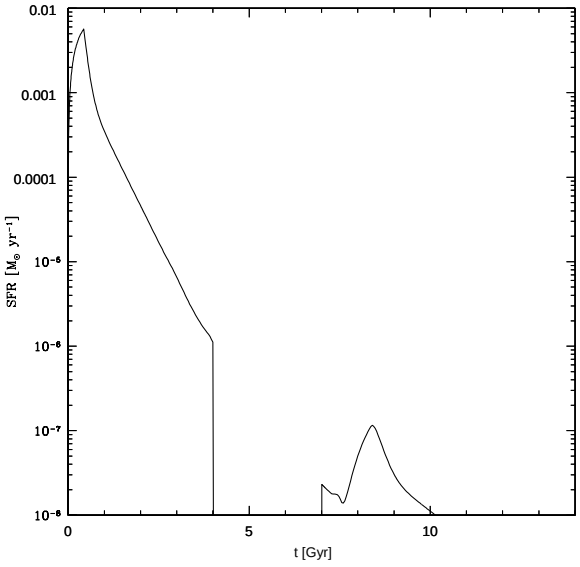

Figure 5. In this Figure we show the Carina SFR (in $M_{\odot}/yr$) as predicted by our model with $\nu = 0.2$ Gyr^{-1} and $\omega = 10$.

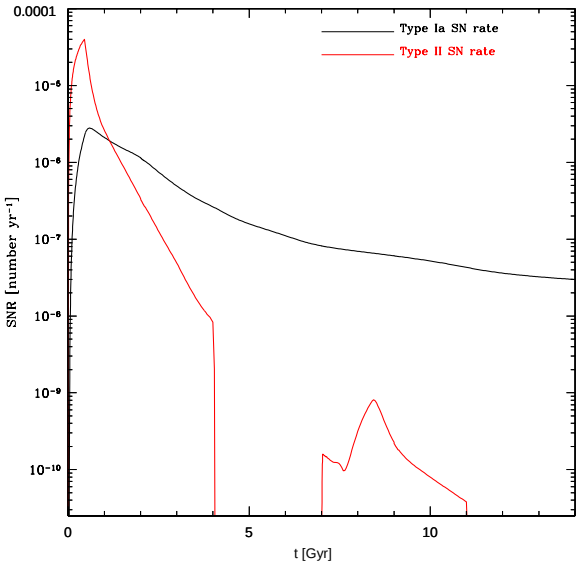

Figure 6. In this Figure we plot the Carina Type II and Type Ia supernova rates predicted by the same model as Fig.(5).

galaxy decreases because of the strong outflow rate. So, at the epoch of the third burst (at 7 Gyr), the intensity of the SFR is much lower than the intensity of the SFR at the end of the second burst (at 4 Gyr), when there was much more gas. Here we did not consider external effects on the SFH (see for this Pasetto et al. 2011).

Fig.(6) shows the SN rates predicted by the best model. We predict a present time SNIa rate of $7.16 \cdot 10^{-4}$ $SNuM$

In Tab.(4), we report the main predictions of all the chemical evolution models which we have performed for the Carina dSph. In the first two columns, we listed the input parameters (ν and ω) characterizing each model. Briefly, by

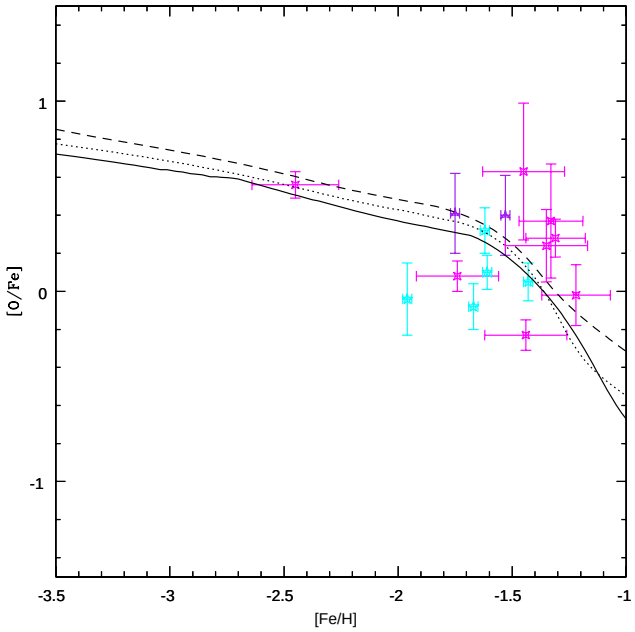

Figure 7. In this Figure, we compare the observed $[O/Fe]$ vs. $[Fe/H]$ abundance ratios of Carina dSph member stars with the trends predicted by our $\omega = 10$ models. The dataset consists of the data samples of Shetrone et al. (2003, in cyan), Koch et al. (2008a, in magenta) and Venn et al. (2012, in purple). The solid line corresponds to the model with $\nu = 0.05$ Gyr^{-1}, the dotted line to the model with $\nu = 0.1$ Gyr^{-1} and the dashed line to the model with $\nu = 0.2$ Gyr^{-1}.

looking at the Table, the reader can note again that enhancing the star formation efficiency ν, for a fixed value of the wind parameter ω, will cause the peak of the MDF to shift towards higher values of $[Fe/H]$, the galactic wind to begin at earlier times, and the total stellar mass at the present time to be larger. Conversely, for a fixed value of the star formation efficiency ν, models with higher values of the wind parameter ω predict the MDF to shift towards lower $[Fe/H]$, and both the stellar and gas masses to be lower at the present time. In order to explain such trends, the same arguments expressed in section 4.1 regarding the Sculptor dSph are also valid here, and we will not repeat them again.

From Tab.(4), all the chemical evolution models we calculated predict both final gas and stellar masses at the present time which are in agreement with the observations ($M_{gas,obs} < 2.1 \cdot 10^2$ $M_{\odot}$ from Grcevich & Putman 2009, and $M_{\star,obs} \approx 1.0 \cdot 10^6$ $M_{\odot}$ from Dekel & Silk 1986).

4.2.1 Carina dSph: abundance ratios and interpretation

Since we adopted low star formation efficiencies, the $[\alpha/Fe]$ ratio is predicted to decrease at very low $[Fe/H]$, and such a decrease steepens even more once the galactic wind starts (see also section 4.1.1). These trends are illustrated in Fig.(7) for the pattern of $[O/Fe]$ vs. $[Fe/H]$ abundance ratios and in Fig.(8) for the calcium, silicon, magnesium and titanium abundance ratios. Especially for the oxygen, there is quite a good agreement between the predictions of our models and the observations.

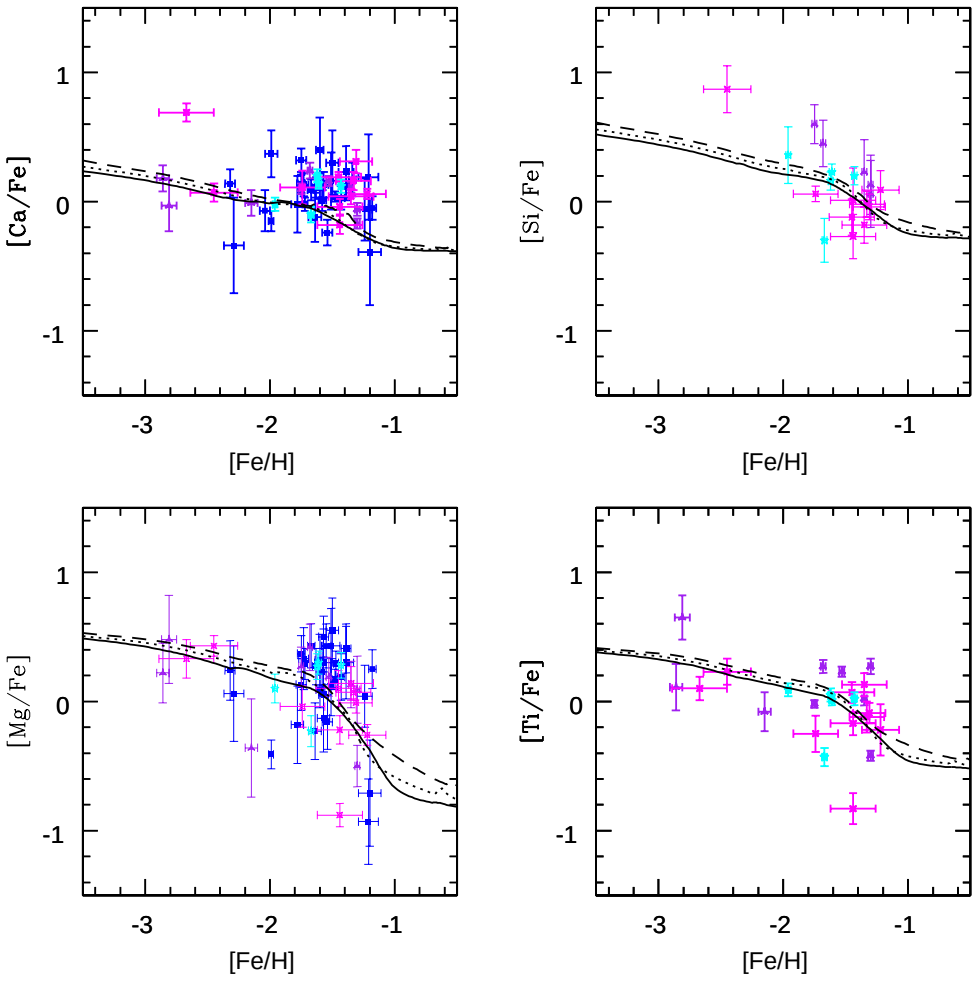

Figure 8. In this Figure, we compare the $[\alpha/Fe]$ vs. $[Fe/H]$ abundance ratios for calcium, silicon, titanium and magnesium as observed in the Carina dSph member stars with the trends predicted by our $\omega = 10$ models. The dataset consists of the data samples of Shetrone et al. (2003, in cyan), Koch et al. (2008a, in magenta), Lemasle et al. (2012, blue) and Venn et al. (2012, in purple). The solid line corresponds to the model with $\nu = 0.05\ Gyr^{-1}$, the dotted line to the model with $\nu = 0.1\ Gyr^{-1}$ and the dashed line to the model with $\nu = 0.2\ Gyr^{-1}$.

4.2.2 Carina dSph: MDF and interpretation

In Fig.(9), we compare the observed stellar MDF with the one predicted by our $\omega = 10$ models. The best matching is given by the model with $\nu = 0.2\ Gyr^{-1}$ and $\omega = 10$. Therefore, star formation in Carina was bursty and characterized by a higher efficiency - and so by lower typical time-scales - than in Sculptor. The most evident effect caused by their different typical star formation time-scales resides in the $[Fe/H]$ of their MDF-peak, which is predicted by the best model for Sculptor ($\nu = 0.05\ Gyr^{-1}$) to be at $[Fe/H] = -1.79$ dex, whereas the Carina best model predicts it at $[Fe/H] = -1.55$ dex.

4.2.3 Carina dSph: previous models

The first detailed chemical evolution model calculated for the Carina dSph was presented in Lanfranchi & Matteucci (2004) and its main basic differences from our models have been summarized in section 4.1.3. They assumed all dSphs to be characterized by the same infall mass and the same mass of DM halo. Conversely, they were able to vary the SFH from galaxy to galaxy, as it was given by the CMD-fitting analysis. They adopted for the Carina dSph a SFH taken from Hernandez et al. (2000), which was not confirmed by later and more accurate observations (Rizzi et al. 2003). Lanfranchi et al. (2006b) adopted the SFH from Rizzi et al. (2003) and were able to reproduce the observed stellar MDF.

The final results of both chemical evolution models of Lanfranchi & Matteucci (2004) and Lanfranchi et al. (2006b) are very similar to the ones found by this work, although they adopted a *differential* galactic wind (Recchi et al. 2001). The best model of Lanfranchi et al. (2006b) has $\nu = 0.14\ Gyr^{-1}$ and $\omega_i = 5$.

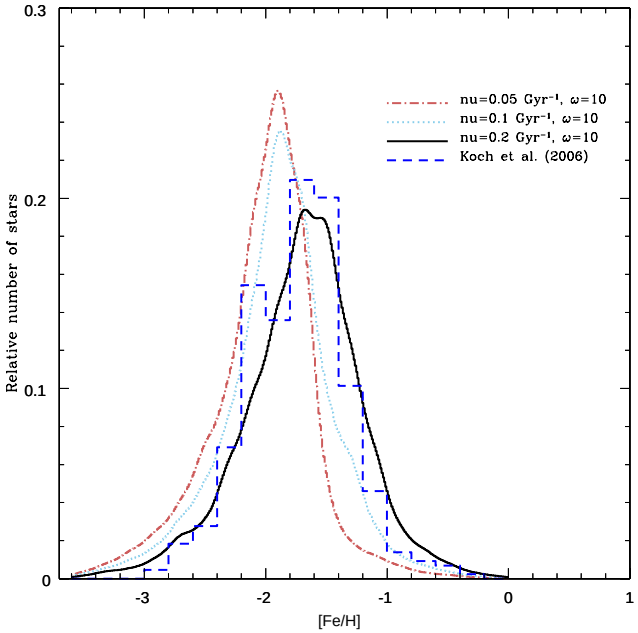

Figure 9. The Figure shows the comparison between the observed stellar MDF in the Carina dSph (data from Koch et al. 2006) and the stellar MDFs predicted by our $\omega = 10$ models. The model which best reproduces the observed MDF is characterized by $\nu = 0.2\ Gyr^{-1}$ and $\omega = 10$.

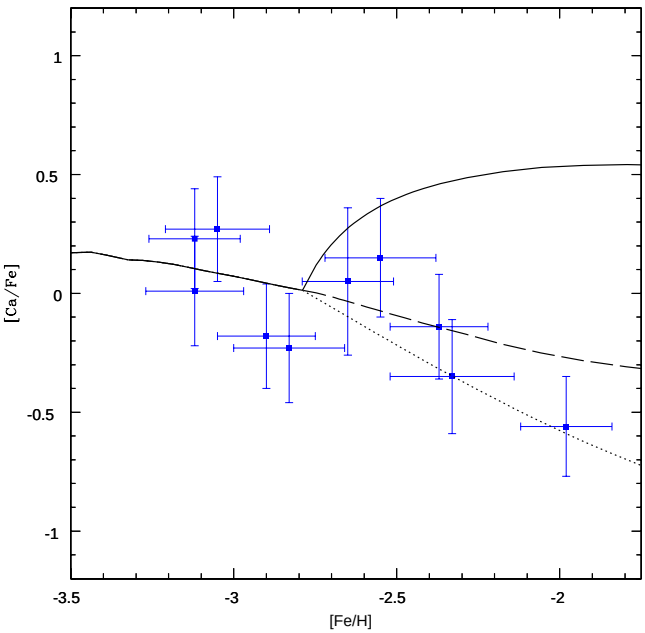

Figure 10. In this Figure, we compare the $[Ca/Fe]$ vs. $[Fe/H]$ trends in Hercules predicted by models with different implemenentations of the galactic wind. The dataset has been taken from Adén et al. (2011). The curve in solid line corresponds to the model with iron-enhanced differential wind (Recchi et al. 2001); the dotted line corresponds to the prediction of the model with α-enhanced differential wind (Marconi et al. 1994) , whereas the dashed line represents the prediction of the model with normal wind. The observed dataset (blue squares with errorbars) are from Adén et al. (2011).

4.3 Chemical evolution of the Hercules UfD

The chemical evolution models we ran for the Hercules UfD adopt the same theoretical prescriptions - and so the same numerical code - as the ones adopted for the dSph galaxies. The mass of the DM halo M_{DM}, the effective radius of the *luminous* (baryonic) component of the galaxy, as well as the SFH of the galaxy have been taken from the observations and kept fixed for all the models. The main difference resides in the fact that UfDs suffered an even slower SFR than dSphs (see also Salvadori & Ferrara 2009).

We assumed for the Hercules UfD a DM halo with mass $M_{DM} = 1.9 \cdot 10^6\ M_{\odot}$ (Adén et al. 2009a). The fraction between the core radius of the DM halo and the effective radius of the baryonic component of the galaxy has been set at $S = \frac{r_L}{r_{DM}} = 0.3$, where the effective radius of the *luminous* (baryonic) component of the galaxy has been assumed to be $r_L = 330\ pc$ (Martin et al. 2008).

Since the CMD-fitting analysis derived a SFH concentrated in the very early epochs of the galaxy evolution (de Jong et al. 2008; Sand et al. 2009), we assumed the galaxy to have formed stars in the first Gyr of its evolution (see Tab.(5). This is the only SFH which allowed us to reproduce all the observed features of the galaxy.

Tab.(5) summarizes the parameters of the most relevant models we calculated for the chemical evolution of the Hercules UfD. We tested models with three different infall masses: $M_{inf} = 1.0$, 2.5, and $5.0 \cdot 10^7\ M_{\odot}$, which have been accreted inside the potential well of the dark matter halo in a very short infall time-scale: $\tau_{inf} = 0.005$ Gyr. This is equivalent to assume that the gas mass is all present since the beginning. The chemical composition of the infalling gas has been assumed to be primordial.

Three different implementations of the galactic wind were tested:

(i) *normal wind*: all the chemical elements are characterized by the same wind parameter ω. This means that the galactic wind expels all the elements with same efficiency.
(ii) *α-enhanced differential wind* (Marconi et al. 1994): the α-elements are expelled by galactic winds with more efficiency than the iron. This means that $\omega_{\alpha} > \omega_{Fe}$. We implemented this galactic wind by adopting: $\omega_{\alpha} = 1.0 \cdot \omega$ and $\omega_{Fe} = 0.3 \cdot \omega$. This can be explained if we assume that massive stars explode in clusters and therefore they transfer more efficiently their energy into the ISM than isolated SNe such as Type Ia ones.
(iii) *Iron-enhanced differential wind* (Recchi et al. 2001): the iron is expelled by galactic winds more efficiently than the α-elements . This means that $\omega_{Fe} > \omega_{\alpha}$. This assumption is based on the fact that SNe Ia explode in a medium already heated and diluted by the previous activity of SNe II, as suggested by Recchi et al. (2001). However, Recchi et al. (2004) have later shown that this conclusion is valid only for an isolated starburst.

In Tab.(6), we report the predictions of our models; the first two columns specify each model in terms of its input parameters M_{inf}, ν, and ω. All the models predict

Hercules: parameters of the models								
ν	ω	τ_{inf}	SFH	M_{inf}	M_{DM}	r_L	$S=\frac{r_L}{r_{DM}}$	IMF
$[Gyr^{-1}]$		[Gyr]	[Gyr]	$M_\odot$	$M_\odot$	$[pc]$		
0.002/0.003/0.005/0.008	10	0.005	$0-1$	$1.0/2.5/5.0\cdot10^7$	$1.9\cdot10^6$	330	0.3	Salpeter (1955)

Table 5. *Table:* we summarize here the specific characteristics of all the chemical evolution models performed for the Boötes I UfD. *Columns:* (1) star formation efficiency; (2) wind parameter; (3) infall time-scale; (4) period of major star formation activity (de Jong et al. 2008; Sand et al. 2009); (5) total infall gas mass; (6) mass of the dark matter halo (Adén et al. 2009a); (7) effective radius of the *luminous* (baryonic) matter (Martin et al. 2008); (8) ratio between the core radius of the dark matter halo and the effective radius of the *luminous* matter; (7) initial mass function.

Hercules chemical evolution models						
Input parameters	Model predictions					
	ν	ω	$M_{\star,fin}$	$M_{gas,fin}$	t_{wind}	$[Fe/H]_{peak}$
	$[Gyr^{-1}]$		$M_\odot$	$M_\odot$	[Gyr]	dex
$M_{inf}=1.0\cdot10^7\ M_\odot$	0.002	10	$0.11\cdot10^5$	$0.35\cdot10^1$	0.97	-3.06
	0.003	10	$0.14\cdot10^5$	$0.49\cdot10^1$	0.76	-3.03
	0.005	10	$0.17\cdot10^5$	$0.18\cdot10^1$	0.56	-2.99
	0.008	10	$0.21\cdot10^5$	$0.82\cdot10^0$	0.41	-2.94
$M_{inf}=2.5\cdot10^7\ M_\odot$	0.002	10	$0.28\cdot10^5$	$0.88\cdot10^1$	2.41	-3.05
	0.003	10	$0.42\cdot10^5$	$0.13\cdot10^2$	1.36	-2.87
	0.005	10	$0.66\cdot10^5$	$0.22\cdot10^2$	0.92	-2.67
	0.008	10	$0.85\cdot10^5$	$0.22\cdot10^2$	0.71	-2.62
$M_{inf}=5.0\cdot10^7\ M_\odot$	0.002	10	$0.55\cdot10^5$	$0.48\cdot10^8$	no wind	-3.05
	0.003	10	$0.85\cdot10^5$	$0.26\cdot10^2$	6.76	-2.87
	0.005	10	$0.14\cdot10^6$	$0.44\cdot10^2$	1.68	-2.65
	0.008	10	$0.22\cdot10^6$	$0.71\cdot10^2$	1.07	-2.43

Table 6. *Table:* we reported for each model with *normal wind* its main predictions. *Columns:* (1) Infall mass; (2) star formation efficiency; (3) wind parameter; (4) predicted actual total stellar mass; (5) predicted actual total gas mass; (6) time of the onset of the galactic wind; (7) peak of the stellar MDF predicted by the models.

a very small total gas mass at the present time, in agreement with the observations ($M_{gas,obs} < 466\ M_\odot$, from Grcevich & Putman 2009). The actual total stellar mass of the galaxy ($M_{\star,obs} = 7.2^{+1.2}_{-1.1}\cdot10^4\ M_\odot$, from Martin et al. 2008) is quite well reproduced by our models. However, we have to stress that such observed quantities remain still rather uncertain at the present time.

All our models predict the MDF to peak at extremely low $[Fe/H]$ abundances. This is an effect both of the very low star formation efficiencies and of the very shallow potential well, which allows the galactic wind to develop earlier and, therefore, to diminish further the SFR in the subsequent evolution of the galaxy. Although we varied the ν parameter within a small range (from $\nu = 0.002\ Gyr^{-1}$ up to $\nu = 0.008\ Gyr^{-1}$), we obtained significant variations in the final predicted features of the galaxy.

As one can see in Tab.(6), diminishing the infall mass M_{inf} will cause the MDF to peak at smaller $[Fe/H]$ values, once the other parameters are fixed. That is because the SFR has been assumed to be proportional to the gas mass inside the galaxy. In fact, the larger the gas mass available, the higher will be the star formation activity; so the chemical enrichment of the ISM will proceed at higher rates, shifting the MDF towards higher $[Fe/H]$.

4.3.1 Hercules UfD: abundance ratios and interpretation

At extremely low $[Fe/H]$, it turns out that $[Ca/Fe]$ in the Hercules UfD steeply decreases from abundances above the solar values ($[Ca/Fe] = +0.32 \pm 0.22$ dex at $[Fe/H] = -3.10 \pm 0.16$ dex) down to $[Ca/Fe] = -0.51 \pm -0,21$ dex at $[Fe/H] = -2.03 \pm 0.14$ dex (Adén et al. 2011). In order to reproduce such a trend, confirmed also by successive observational spectroscopic studies of UfD stars (Gilmore et al. 2013; Vargas et al. 2013), we tested a formation scenario characterized by a very short infall time-scale ($\tau_{inf} = 0.005$ Gyr) and very low star formation efficiencies ($0.003\ Gyr^{-1} \leqslant \nu \leqslant 0.008\ Gyr^{-1}$), even lower than for dSphs and in agreement with previous studies (Salvadori & Ferrara 2009). The short infall time-scale gives rise to an enhanced SFR in the earliest stages of galaxy evolution, during which large amounts of α-elements were likely to be ejected by Type II SN explosions into the ISM, whereas the extremely low star formation efficiency produces a very slow growth of the $[Fe/H]$; so when SNe Ia occur, the $[Fe/H]$ is still very low and the $[Ca/Fe]$ steeply decreases.

In Fig.(10), we show the effect of the various wind implementations on the $[Ca/Fe]$ vs. $[Fe/H]$ diagram. An iron-enhanced *differential wind* is not able to reproduce the ob-

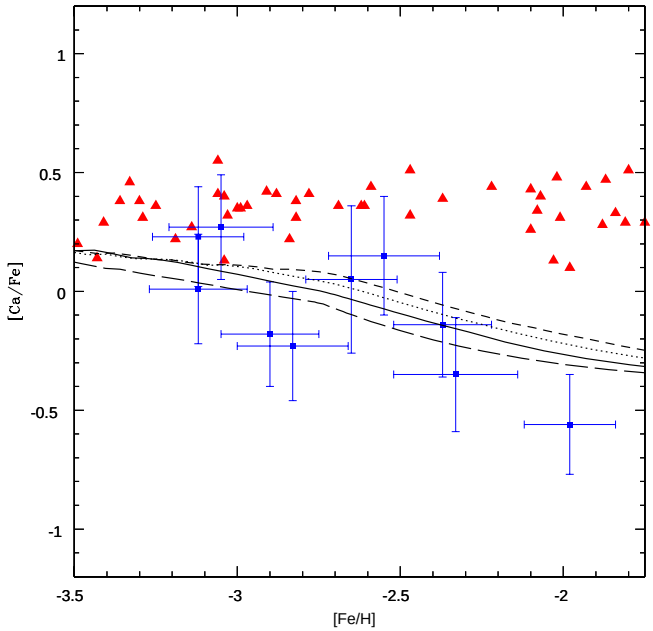

Figure 11. In this Figure, we compare the $[Ca/Fe]$ vs. $[Fe/H]$ abundance pattern as observed in the Hercules UfD member stars (data from Adén et al. 2011) with the predictions of our models with $\omega = 10$ (normal wind) and $M_{inf} = 1.0 \cdot 10^7\ M_{\odot}$. We show also the abundance pattern of $[Ca/Fe]$ vs. $[Fe/H]$ as observed in Galactic halo stars (red triangles, data from Gratton et al. 2003; Reddy et al. 2003; Cayrel et al. 2004; Reddy et al. 2006). The prediction of the model with $\nu = 0.002\ Gyr^{-1}$ is in long dashed line; the model with $\nu = 0.003\ Gyr^{-1}$ is in solid line; the model with $\nu = 0.005\ Gyr^{-1}$ is illustrated in dotted line, whereas the model with $\nu = 0.008\ Gyr^{-1}$ is represented by the dashed line. By looking at this Figure, it is clear that Hercules UfD member stars suggest different trend of $[Ca/Fe]$ as a function of $[Fe/H]$.

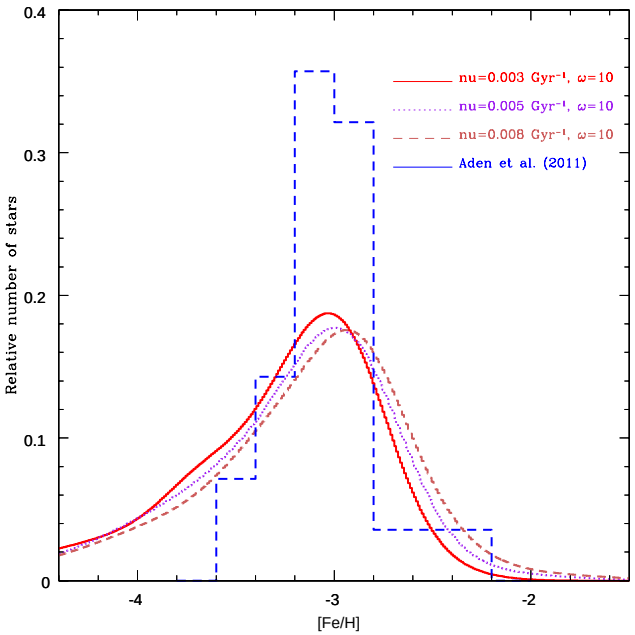

Figure 12. In this Figure, we show the comparison between the observed stellar MDF of the Hercules UfD (data from Adén et al. 2011) and the predictions of our models with $\omega = 10$ (normal wind) and $M_{inf} = 1.0 \cdot 10^7\ M_{\odot}$. The dataset is built up on a sample of only 28 RGB stars, with $[Fe/H]$ values in a very tight range, between $[Fe/H] = -3.1$ dex and $[Fe/H] = -2.9$ dex and very low relative numbers of stars in the other bins towards both lower and higher $[Fe/H]$ abundances. The MDF predicted by our models are based on a large number of artificial stars, according to the SFH and to the IMF assumed. We are not able to reproduce the height of the observed-MDF peak. Our choice of the best model is oriented towards the model which reproduces the $[Fe/H]_{peak}$ abundance of the observed MDF, which turns out to have $\nu = 0.003\ Gyr^{-1}$ and $\omega = 10$.

served steep decrease in $[Ca/Fe]$ vs. $[Fe/H]$. Conversely, models with normal and α-enhanced differential wind agree with the observations. By looking at this Figure, the three models predict the galactic wind to start at the same time. In fact, by fixing the τ_{inf} and M_{inf} parameters, the time of the galactic wind onset depends only upon the features of the galaxy potential well (which affects the binding energy of the gas) and upon the SFH of the galaxy (which affects the computation of the thermal energy of the ISM). Therefore, the only parameter affecting the time of onset of the galactic wind is the ν parameter, whereas the ω parameter, as well as its particular implementation, comes into play only after the wind has started. An iron-enhanced differential wind predicts the $[Ca/Fe]$ to increase as $[Fe/H]$ grows, soon after the wind onset, at variance with observations. In fact, while SNe Ia enrich the ISM with large amounts of iron, causing the $[Fe/H]$ in the ISM to grow with time, the iron is also expelled by the galactic wind with higher efficiency than the α-elements as the calcium.

Since we do not still have evidences of galactic outflows enriched in α-elements, we preferred as best models those with normal galactic wind.

In Fig.(11), we show the effect of changing the ν parameter on the $[Ca/Fe]$ vs. $[Fe/H]$ diagram, with $\omega = 10$ (normal wind) and $M_{inf} = 1.0 \cdot 10^7\ M_{\odot}$. The model which best reproduces the overall trend suggested by the dataset is characterized by $\nu = 0.003\ Gyr^{-1}$ and $\omega = 10$. In this Figure, we report also the observed $[Ca/Fe]$ vs. $[Fe/H]$ abundance pattern of Galactic halo stars. Although more data are necessary, Hercules UfD stars and Galactic halo stars display different trends of $[Ca/Fe]$ vs. $[Fe/H]$. In particular, halo stars do not share the fast decline in $[\alpha/Fe]$ exhibited by the stars in Hercules. This fact seems to rule out the hypothesis that UfDs would have been the building blocks of the stellar halo of the Milky Way. In fact, models (e.g. Brusadin et al. 2013) suggest that the Galactic halo have formed on a timescale of ≈ 0.2 Gyr with a SF efficiency $\nu = 0.2\ Gyr^{-1}$ and $\omega \simeq 14$.

4.3.2 Hercules UfD: MDF and interpretation

The observed stellar MDF (Adén et al. 2011) is built up on a very poor statistical sample, which consists of only 28 RGB stars - the most luminous ones - previously identified and studied by Adén et al. (2009b). It turns out that most of the stars in the Adén et al. (2011) sample resides in a

Boötes I: parameters of the models								
ν	ω	τ_{inf}	SFH	M_{inf}	M_{DM}	r_L	$S = \frac{r_L}{r_{DM}}$	IMF
$[Gyr^{-1}]$		[Gyr]	[Gyr]	$M_\odot$	$M_\odot$	$[pc]$		
0.002/0.005/0.01/0.05	10/15	0.005	$0-4$	$1.0/2.5/5.0 \cdot 10^7$	$0.30 \cdot 10^7$	242	0.2	Salpeter (1955)

Table 7. *Table:* we summarize here the specific characteristics of all the chemical evolution models performed for the Boötes I UfD. *Columns:* (1) star formation efficiency; (2) wind parameter; (3) infall time-scale; (4) period of major star formation activity (de Jong et al. 2008); (5) total infall gas mass; (6) mass of the dark matter halo (Collins et al. 2013); (7) effective radius of the *luminous* (baryonic) matter (Martin et al. 2008); (8) ratio between the core radius of the dark matter halo and the effective radius of the *luminous* matter; (7) initial mass function.

Boötes I chemical evolution models						
Input parameters	Model predictions					
	ν	ω	$M_{\star,fin}$	$M_{gas,fin}$	t_{wind}	$[Fe/H]_{peak}$
	$[Gyr^{-1}]$		$M_\odot$	$M_\odot$	[Gyr]	dex
$M_{inf} = 1.0 \cdot 10^7\ M_\odot$	0.002	10	$0.14 \cdot 10^5$	$0.35 \cdot 10^1$	1.17	-2.99
	0.005	10	$0.21 \cdot 10^5$	$0.50 \cdot 10^1$	0.68	-2.91
	0.01	10	$0.29 \cdot 10^5$	$0.14 \cdot 10^1$	0.45	-2.81
	0.05	10	$0.68 \cdot 10^5$	$0.68 \cdot 10^0$	0.16	-2.55
$M_{inf} = 2.5 \cdot 10^7\ M_\odot$	0.002	10	$0.58 \cdot 10^5$	$0.90 \cdot 10^1$	2.01	-2.68
	0.005	10	$0.75 \cdot 10^5$	$0.57 \cdot 10^2$	2.65	-2.69
	0.01	10	$0.11 \cdot 10^6$	$0.39 \cdot 10^2$	0.76	-2.51
	0.05	10	$0.25 \cdot 10^6$	$0.55 \cdot 10^1$	0.29	-2.31
$M_{inf} = 5.0 \cdot 10^7\ M_\odot$	0.002	10	$0.19 \cdot 10^6$	$0.19 \cdot 10^2$	3.21	-2.39
	0.005	10	$0.25 \cdot 10^6$	$0.45 \cdot 10^2$	1.72	-2.34
	0.01	10	$0.33 \cdot 10^6$	$0.89 \cdot 10^2$	1.12	-2.28
	0.05	10	$0.70 \cdot 10^6$	$0.35 \cdot 10^2$	0.44	-2.06

Table 8. *Table:* we reported for each model its main predictions. *Columns:* (1) wind parameter; (2) star formation efficiency; (3) predicted actual total stellar mass; (4) predicted actual total gas mass; (5) time of the onset of the galactic wind; (6) peak of the stellar MDF predicted by the models.

very tight metallicity range, between $[Fe/H] = -3.1$ dex and $[Fe/H] = -2.9$ dex, with very low relative numbers of stars in the other bins towards both lower and higher $[Fe/H]$ abundances. Conversely, our predicted stellar MDF is based upon a very large number of *artificial* stars determined from the assumed SFR and IMF. So, when we normalize the number of stars counted in a specific $[Fe/H]$-bin to the total number of stars, the height of the peak in the observed stellar MDF turns always out much higher than the more "populated" and dispersed MDF of our models.

In Fig.(12), we have reported the comparisons between the observed MDF and our models with $M_{inf} = 1.0{\cdot}10^7\ M_\odot$. By looking at the Figure, the only model matching the observations is characterized by a star formation efficiency $\nu = 0.003\ Gyr^{-1}$; it is able to reproduce the $[Fe/H]$-position of the peak, as well as the width of the observed MDF, although it predicts a rather large relative number of stars in the extremely low $[Fe/H]$-wing, which spectroscopic observations have not yet been able to cover, because of the extremely low flux coming from those UfD member stars and the still relative low signal-to-noise ratio affecting the observations. By supposing that at extremely low $[Fe/H]$ abundances a hypothetical previous very massive population of stars might have enriched the medium with metals, the predicted relative number of stars with very low $[Fe/H]$ could be diminished, as it was similarly suggested in the past for solving the so-called *G- dwarf problem* in the solar neighborhood. In this work, we only envisaged this hypothesis but we did not test its validity. Finally, by supposing that the chemical composition of the initial infall gas mass is not primordial but rather pre-enriched with metals by a previous population of stars, the observed enhanced α-element abundances at extremely low $[Fe/H]$ might be explained. In fact, this might increase the initial metal content within the ISM and allow to build up that "common *metallicity floor*" to all the various different galaxy types, as suggested by Ferrara (2012).

Our best model for Hercules requires $\nu = 0.003\ Gyr^{-1}$, $\omega = 10$ and $M_{inf} = 1.0 \cdot 10^7\ M_\odot$.

4.4 Chemical evolution of the Boötes I UfD

We assumed for the Boötes I UfD a dark matter halo with mass $M_{DM} = 0.30 \cdot 10^7\ M_\odot$ (Collins et al. 2013). The ratio between the core radius of the DM halo and the effective radius of the galaxy baryonic component has been assumed to be $S = \frac{r_L}{r_{DM}} = 0.2$, where the effective radius of the baryonic (*luminous*) component of the galaxy

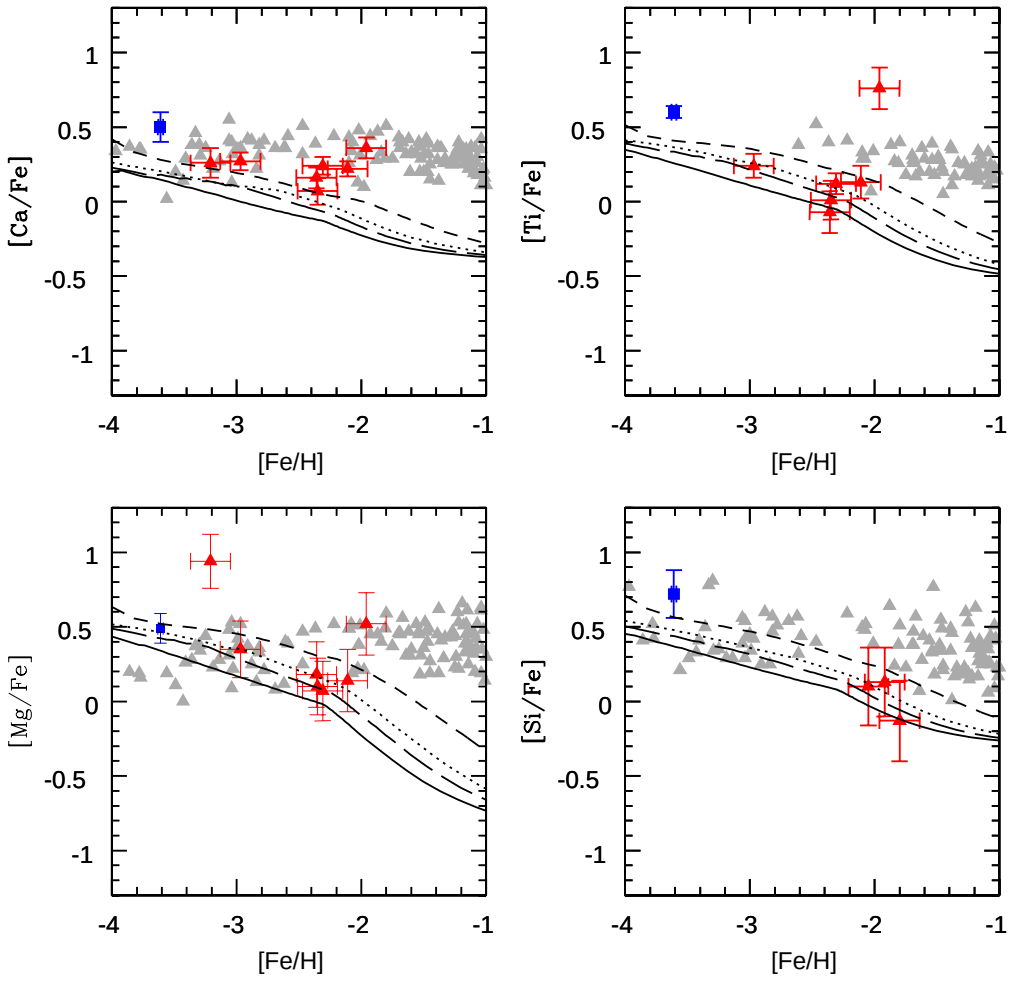

Figure 13. In this Figure, we compare the $[\alpha/Fe]$ vs. $[Fe/H]$ abundance ratios for calcium, silicon, titanium and magnesium as observed in the Boötes I UfD member stars with the trends predicted by our models with $\omega = 10$ (normal wind) and $M_{inf} = 2.5 \cdot 10^7\ M_{\odot}$. The dataset consists of the data samples of Norris et al. (2010, blue squares) and Gilmore et al. (2013, red triangles) ("NY" analysis, from Norris et al. 2010). The model with $\nu = 0.002\ Gyr^{-1}$ is given by the solid line; the model with $\nu = 0.005\ Gyr^{-1}$ is given by the long dashed line, whereas the model with $\nu = 0.01\ Gyr^{-1}$ is represented by the dotted line. Eventually, the model with $\nu = 0.05\ Gyr^{-1}$ is represented by the dashed line. We show also the abundance patterns of $[\alpha/Fe]$ vs. $[Fe/H]$ as observed in Galactic halo stars (grey triangles, data from Gratton et al. 2003; Reddy et al. 2003; Cayrel et al. 2004; Reddy et al. 2006).

is $r_L = 242\ pc$ (Martin et al. 2008). The SFH has been assumed to be made of only one episode lasting 4 Gyr, from 0 up to 4 Gyr (de Jong et al. 2008).

The infall mass of primordial gas from which the galaxy formed by accretion has been varied; we tested models with $M_{inf} = 1.0$, 2.5 and $5.0 \cdot 10^7\ M_{\odot}$. The infall time-scale of such initial reservoir of gas has been assumed to be very short, $\tau_{inf} = 0.005$ Gyr. In Tab.(7), we reported the parameters of our Boötes I chemical evolution models. All the models are characterized by a *normal* galactic wind.

In Tab.(8), we report the main predictions of our chemical evolution models. In the first two columns, we listed the input parameters: M_{inf} and ν. From the Table, the lower the star formation efficiency ν - as well as the lower the infall mass M_{inf} - the lower will be the $[Fe/H]$ at which the stellar MDF has its peak. Our models predict extremely low total gas content at the present time, as well as much lower total stellar mass than in dSph galaxies. This is again an effect both of the low initial infall gas mass and of the very low star formation efficiencies. The predicted final total gas masses are in agreement with the observed values ($M_{gas,obs} < 86\ M_{\odot}$, from Grcevich & Putman 2009), as well as the predicted final total stellar masses agree quite well with the observed value $M_{\star,obs} = (6.7 \pm 0.6) \cdot 10^4\ M_{\odot}$, from Martin et al. (2008), which is however very uncertain since it was inferred from a poor number of hypothetical stars belonging to the galaxy: $N_{\star} = 324^{+28}_{-23}$, derived by means of a maximum likelihood algorithm applied to SDSS data. Furthermore, the observed total stellar mass strongly depends also on the IMF adopted and here we report the quantity derived by Martin et al. (2008) when using the Salpeter (1955) IMF.

4.4.1 Boötes I UfD: abundance ratios and interpretation

In order to reproduce the $[\alpha/Fe]$ vs. $[Fe/H]$ observed trends (Gilmore et al. 2013; Norris et al. 2010), which are indeed rather uncertain, we adopted a very short infall time-scale - which enhances the SFR in the earliest stages of the galaxy evolution, giving rise to high $[\alpha/Fe]$ abundances at extremely low $[Fe/H]$ - coupled with very low star formation efficiencies - which cause the decrease in the α-element abundances to start at very low $[Fe/H]$. We show our results in Fig. (13), where we compare our theoretical curves with the observed dataset of the $[\alpha/Fe]$ vs. $[Fe/H]$ abundance patterns for calcium, silicon, titanium and magnesium. In this Figure, we compare also the chemical abundances of Boötes I UfD member stars with those of Galactic halo stars.

The best agreement with the observed dataset is obtained by the model with $\nu = 0.01\ Gyr^{-1}$, $\omega = 10$ and $M_{inf} = 2.5 \cdot 10^7\ M_{\odot}$. At extremely low $[Fe/H]$, the stars of Boötes I display enhanced $[Ca/Fe]$ abundance ratios. Although our theoretical curves are able to reproduce the titanium, magnesium and silicon abundance patterns, there is still a discrepancy with calcium. That is probably due to the large uncertainty in the calcium yields from massive stars.

4.4.2 Boötes I UfD: MDF and interpretation

The observed stellar MDF has been taken from Lai et al. (2011). Originally, their data sample was constituted by low-resolution spectra of 25 stars, which then was extended to 41 stars by adding non-overlapping stars from Norris et al. (2010) and Feltzing et al. (2009). This gave rise to an inhomogeneous collection of datasets, which is also a rather poor statistical sample.

As in the case of the Hercules stellar MDF (see section 4.3.2), also here we are not able to reproduce the height of the observed MDF-peak. This is clearly illustrated in Fig.(14), where we also show that the only model able to reproduce the peak and the width of the observed MDF is characterized by $\nu = 0.01\ Gyr^{-1}$, $\omega = 10$ and $M_{inf} = 2.5 \cdot 10^7\ M_{\odot}$.

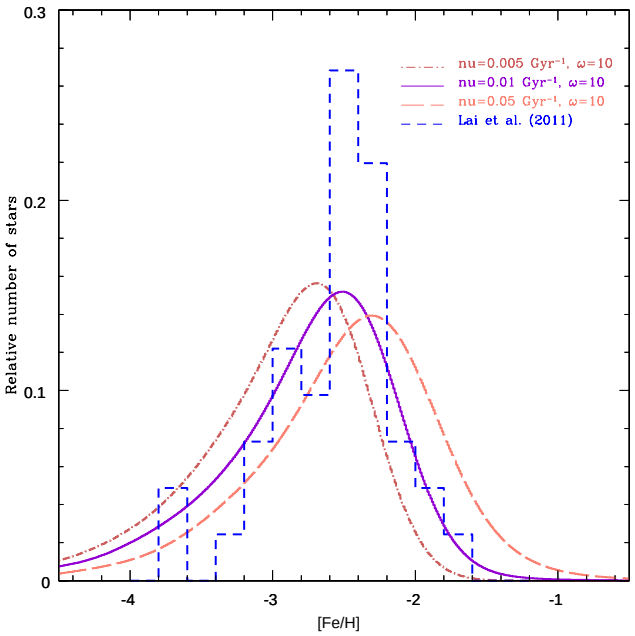

Figure 14. In this Figure, we show the comparison between the observed stellar MDF of the Boötes I UfD (data from Lai et al. 2011) and the predictions of our models with $\omega = 10$ (normal wind) and $M_{inf} = 2.5 \cdot 10^7\ M_{\odot}$. Again, as in the case of the Hercules UfD, the dataset is built up on a sample of only 41 stars, highly concentrated in a very tight $[Fe/H]$ range. We are not able to reproduce the height of the observed-MDF peak. The model which best reproduces the $[Fe/H]_{peak}$ abundance of the observed MDF turns out to have $\nu = 0.01\ Gyr^{-1}$ and $\omega = 10$.

5 CONCLUSIONS

5.0.3 Summary on dSph chemical evolution

In this paper, we have assumed that dSph galaxies form by accretion of an *infall mass* of $M_{inf} = 1.0 \cdot 10^8\ M_{\odot}$ with primordial chemical composition. The infall rate obeys to a decaying exponential law with an *infall time- scale* $\tau_{inf} = 0.5$ Gyr. The mass content and the core radius of the DM halo have been taken from the observations. In particular, here we modeled Sculptor and Carina and our results can be summarized as follows.

(i) Only by assuming low star formation efficiencies ($\nu = 0.05 - 0.5\ Gyr^{-1}$) relative to the Milky Way ($\nu \sim 1\ Gyr^{-1}$ in the solar vicinity, Chiappini et al. 1997), we have been able to explain the decline in the $[\alpha/Fe]$ abundance ratios observed at very low $[Fe/H]$. In fact, the lower the ν parameter, the lower is the amount of iron produced by Type II SNe; this causes the $[Fe/H]$ of the ISM, at which Type Ia SNe become predominant in the iron pollution, to be lower. This precisely determines the decrease in the $[\alpha/Fe]$ at very low $[Fe/H]$. This is due to the fact that most of α-elements originates in Type II SNe whereas most of Fe originates in Type Ia SNe exploding on a large range of times (time-delay model).
(ii) Low star formation efficiencies increase the star formation time-scales, giving rise to stellar MDFs peaked towards very low $[Fe/H]$, in very good agreement with the observations indicating that dSphs are very metal-poor stellar systems.
(iii) Galactic winds - driven by SN explosions - play a relevant role in the dSph chemical evolution. We adopted for dSphs a *normal* wind, i.e. a wind with an efficiency equal for all the chemical elements. The net effect of the galactic wind is to diminish further the SFR and cause the $[\alpha/Fe]$ to follow a steeper decline as $[Fe/H]$ increases. Thanks to the strong outflow rates, our models predict very low final total gas masses, according to observations.
(iv) Only by adopting star formation episodes occurring far beyond the reionization epoch, our models were able to build up final total stellar masses of the same order of magnitude as the observed ones ($M_{star,obs} \sim 10^6\ M_{\odot}$), and they could also reproduce the other observed features of dSph galaxies. Our assumptions were based on the results of the CMD-fitting analysis, which have been able, in the past few years, to derive the SFH of many dwarf galaxies of the Local Group.
(v) We adopted the Salpeter (1955) IMF for all the models.

In a recent paper, McWilliam et al. (2013) suggested that to explain the abundance data in Sagittarius an IMF with a lower fraction of massive stars than a Salpeter-like IMF should be preferred. However, by testing an IMF with a steeper slope in the massive star range, we found a neglibible difference in our results.
(vi) Our best models are in good agreement with the previous works (Lanfranchi & Matteucci 2004; Lanfranchi et al. 2006b) and confirm their goodness. Our best model for Sculptor requires $\nu = 0.05\ Gyr^{-1}$ and $\omega = 10$, whereas our best model for Carina requires $\nu = 0.2\ Gyr^{-1}$ and $\omega = 10$.

5.0.4 Summary on UfD chemical evolution

We modeled Hercules and Boötes I, by adopting the same numerical code of dSphs but with different characteristic input parameters. In what follows, we summarize the main features of our UfD chemical evolution models:

(i) Since UfDs are known today to be the faintest and most DM dominated galaxies, we adopted *infall masses* $M_{inf} = (1.0 - 5.0) \cdot 10^7\ M_{\odot}$, which are lower than the ones assumed for dSphs and supported by observations. Such initial reservoir of gas, with primordial chemical composition, was accreted in the galaxy DM halo on a very short typical time-scale ($\tau_{inf} = 0.005$ Gyr).
(ii) Our best model for Hercules requires $\nu = 0.003\ Gyr^{-1}$, $\omega = 10$, $M_{inf} = 1.0 \cdot 10^7\ M_{\odot}$ and $\tau_{inf} = 0.005$ Gyr, whereas our best model for Boötes I requires $\nu = 0.01\ Gyr^{-1}$, $\omega = 10$, $M_{inf} = 2.5 \cdot 10^7\ M_{\odot}$ and $\tau_{inf} = 0.005$ Gyr.
(iii) The $[\alpha/Fe]$ abundance ratios are observed to steeply decrease at very low $[Fe/H]$. This is clearly a signature of very low star formation efficiencies ($\nu = 0.001 - 0.01\ Gyr^{-1}$), even lower than for the dSph ones ($\nu \approx 0.05 - 0.5\ Gyr^{-1}$). In fact, Type Ia SNe start to dominate in the iron pollution of the ISM when the $[Fe/H]$ of the ISM is still very low. This result is in agreement with the previous studies of UfD galaxies, such as Salvadori & Ferrara (2009)
(iv) The very low adopted star formation efficiencies cause the stellar MDFs to be peaked at very low $[Fe/H]$, in very good agreement with observations.
(v) From the CMD-fitting analysis, as well as from the study of the pulsation and metallicity properties of their variable stars, UfDs host very old stellar populations, with ages $> 10 - 12$ Gyr. So, we assumed them to have undergone star formation only in the first gigayears of their chemical evolution history. This fact, coupled with the very low star formation efficiencies, causes the building up of very low final total stellar masses $M_{\star,fin} \sim 10^4 - 10^5\ M_{\odot}$, which are much lower than the observed dSph ones, and in agreement with observational values.
(vi) The actual total gas masses in UfDs are negligible or even undetected. This is a clear evidence of intense galactic winds, which are efficient in the gas removal from the galaxy potential well and started very soon in the galaxy evolution. We tested models with *normal wind*, α-enhanced *differential wind*, and iron-enhanced *differential wind*. All such models agree in predicting negligible final total gas masses but each of them has a different effect in the $[\alpha/Fe]$ vs. $[Fe/H]$ diagram.
(vii) Both *normal* and α-enhanced galactic winds predict a trend of the $[\alpha/Fe]$ vs. $[Fe/H]$ diagram which well agrees with observations. On the other hand, an iron-enhanced *differential wind* predicts the $[\alpha/Fe]$ to increase as $[Fe/H]$ grows once the galactic wind has started, at variance with observations. We suggest the galactic wind to be normal with an efficiency $\omega = 10$, which is the same value adopted in this work for reproducing the main properties of dSph galaxies.
(viii) Our chemical evolution models have been able to reproduce, at the same time and reasonably well, all the observed features of the two UfD galaxies studied, such as the abundance ratio patterns of the α-elements, the stellar MDF, and the total stellar and gas masses at the present time. From the main characteristics of our chemical evolution models and from the observed trend of the UfD chemical abundances, we suggest that the hypothesis that UfDs would have been the survived "building blocks" of the Milky Way halo is unlikely, since the two seem to have undergone very different galactic chemical enrichment histories. In particular, the Galactic halo abundance pattern suggests more vigorous star formation and galactic wind, together with a longer time-scale of gas accretion (see Brusadin et al. 2013). However, more data on UfDs are necessary before drawing firm conclusions.

ACKNOWLEDGMENTS

F.M. acknowledges financial support from PRIN-MIUR 2010-2011 project "The Chemical and Dynamical Evolution of the Milky Way and Local Group Galaxies", prot. 2010LY5N2T. F.V. and F.M. thank M. Nonino, A. Koch and D. Romano for useful suggestions and interesting discussions. We thank an anonymous referee for his/her suggestions.

References

Adén D., Wilkinson M. I., Read J. I., et al., 2009a, ApJ, 706, L150
Adén D., Feltzing S., Koch A., et al., 2009b, A&A, 506, 1147
Adén D., Eriksson K., Feltzing S., et al., 2011, A&A, 525, A153
Asplund M., Grevesse N., Sauval A. J., Scott P., 2009, ARA&A, 47, 481
Battaglia G., Irwin M., Tolstoy E., et al., 2008a, MNRAS, 383, 183
Battaglia G., Helmi A., Tolstoy E., et al., 2008b, ApJ, 681, L13
Belokurov V., Zucker D. B., Evans N. W., et al., 2006, ApJ, 647, L111
Belokurov V., Zucker D. B., Evans N. W., et al., 2007, ApJ, 654, 897
Belokurov V., Walker M. G., Evans N. W., et al., 2010, ApJ, 712, L103
Belokurov V., 2013, NAR, 57, 100
Bradamante F., Matteucci F., D'Ercole A., 1998, ApJ, 337, 338
Brown T. M., Tumlinson J., Geha M., et al., 2013, arXiv:1310.0824

Brusadin G., Matteucci F., Romano D., 2013, A&A, 554, A135
Bullock J. S., Kravtsov A. V., Weinberg D. H., 2001, ApJ, 548, 33
Bullock J. S., Johnston K. V., 2005, ApJ, 635, 931
Cannon R. D., Hawarden T. G., Tritton S. B., 1977, MNRAS, 180, 81P
Catelan M., 2009, ApSS, 320, 261
Cayrel R., Depagne E., Spite M., et al., 2004, A&A, 416, 1117
Cescutti G., François P., Matteucci F., Cayrel R., Spite M., 2006, A&A, 448, 557
Cescutti G., Matteucci F., Lanfranchi G. A., McWilliam A., 2008, A&A, 491, 401
Chabrier G., 2003, PASP, 115, 763
Chiappini C., Matteucci F., Gratton R., 1997, ApJ, 477, 765
Chieffi A., Limongi M., 2013, ApJ, 764, 21
Collins M. L. M., Chapman S. C., Rich R. M., et al., 2013, arXiv:1309.3053
Cooke R., Pettini M., Steidel C. C., Rudie G. C., Jorgenson R. A., 2011, MNRAS, 412, 1047
Cooke R., Pettini M., Steidel C. C., Rudie G. C., Nissen P. E., 2011, MNRAS, 417, 1534
Dall'Ora M., Ripepi V., Caputo F., et al., 2003, AJ, 126, 197
de Boer T. J. L., Tolstoy E., Hill V., et al., 2012, A&A, 539, A103
de Jong J. T. A., Rix H. W., Martin N. F., et al., 2008, AJ, 135, 1361
Dekel A., Silk J., 1986, ApJ, 303, 39
Feltzing S., Eriksson K., Kleyna J., Wilkinson M. I., 2009, A&A, 508, L1
Ferrara A., 2012, American Institute of Physics Conference Series, 1480, 317
François P., Matteucci, F., Cayrel R., et al., 2004, ApJ, 421, 613
Frebel A., Kirby E. N., Simon J. D., 2010, Nature, 464, 72
Frebel A., Bromm V., 2012, ApJ, 759, 115
Gilmore G., Wilkinson M. I., Wyse R. F. G., et al., 2007, ApJ, 663, 948
Gilmore G., Norris J. E., Monaco L., et al., 2013, ApJ, 763, 61
Gratton R. G., Carretta E., Claudi R., Lucatello S., Barbieri M., 2003, A&A, 404, 187
Grcevich J., Putman M. E., 2009, ApJ, 696, 385
Grebel E. K., 1997, Reviews in Modern Astronomy, 10, 29
Harding P., Morrison H. L., Olszewski E. W., et al., 2001, AJ, 122, 1397
Helmi A., White S. D. M, 1999, MNRAS, 307, 495
Helmi A., Irwin M. J., Tolstoy E., et al., 2006, ApJ, 651, L121
Hernandez X., Gilmore G., Valls-Gabaud D., 2000, MNRAS, 317, 831
Hurley-Keller D., Mateo M., Nemec J., 1998, AJ, 115, 1840
Ishigaki M. N., Aoki W., Arimoto N., Okamoto S., 2014, arXiv:1401.1265
Iwamoto K., Brachwitz F., Nomoto K., et al., 1999, ApJ, 125, 439
Keller S. C., Bessell M. S., Frebel A., et al., 2014, Nature, 506, 463
Kirby E. N., Guhathakurta P., Bolte M., Sneden C., Geha M. C., 2009, ApJ, 705, 328
Kirby E. N., Guhathakurta P., Simon J. D., et al., 2010, ApJS, 191, 352
Kirby E. N., Cohen J. G., 2012, AJ, 144, 168
Koch A., Grebel E. K., Wyse R. F. G., et al., 2006, ApJ, 131, 895
Koch A., Grebel E. K., Gilmore G. F., et al., 2008, ApJ, 135, 1580
Koch A., McWilliam A., Grebel E. K., Zucker D. B., Belokurov V., 2008, ApJL, 688, L13
Koch A., 2009, Astronomische Nachrichten, 330, 675
Koch A., Feltzing S., Adén D., Matteucci F., 2013, A&A, 554, A5
Koch A., Matteucci F., Feltzing S., 2012, American Institute of Physics Conference Series, 1480, 190
Lai D. K., Lee Y. S., Bolte M., et al., 2011, ApJ, 738, 51
Lanfranchi G.A., Matteucci F., 2004, MNRAS, 351, 1338
Lanfranchi G. A., Matteucci F., Cescutti G., 2006a, MNRAS, 365, 477
Lanfranchi G. A., Matteucci F., Cescutti G., 2006b, A&A, 453, 67
Lanfranchi G. A., Matteucci F., 2007, A&A, 468, 927
Lanfranchi G. A., Matteucci F., Cescutti G., 2008, A&A, 481, 635
Lanfranchi G. A., Matteucci F., 2010, A&A, 512, A85
Lemasle B., Hill V., Tolstoy E., et al., 2012, A&A, 538, A100
Li W., Chornock R., Leaman J., et al., 2011, MNRAS, 412, 1473
Marconi G., Matteucci F., Tosi M., 1994, MNRAS, 270, 35
Martin N. F., de Jong J. T. A., Rix H.-W., 2008, ApJ, 684, 1075
Mateo M. L., 1998, ARA&A, 36, 435
Matteucci F., Brocato E., 1990, ApJ, 365, 539
Matteucci F., 2001, Astrophysics and Space Science Library, 253
Matteucci F., Recchi S., 2001, ApJ, 558, 351
McWilliam A., Wallerstein G., Mottini M., 2013, ApJ, 778, 149
Monelli M., Pulone L., Corsi C. E., et al., 2003, AJ, 126, 218
Norris J. E., Yong D., Gilmore G., Wyse R. F. G., 2010, ApJ, 711, 350
Norris J. E., Wyse R. F. G., Gilmore G., et al., 2010, ApJ, 723, 1632
Okamoto S., Arimoto N., 2012, Galactic Archaeology: Near-Field Cosmology and the Formation of the Milky Way, 458, 283
Pasetto S., Grebel E. K., Berczik P., Chiosi C., Spurzem R., 2011, A&A, 525, A99
Recchi S., Matteucci F., D'Ercole A., 2001, MNRAS, 322, 800
Recchi S., Matteucci F., D'Ercole A., Tosi M., 2002, A&A, 384, 799
Recchi S., Matteucci F., D'Ercole A., Tosi, M., 2004, A&A, 426, 37
Reddy B. E., Tomkin J., Lambert D. L., Allende Prieto C., 2003, MNRAS, 340, 304
Reddy B. E., Lambert D. L., Allende Prieto C., 2006, MNRAS, 367, 1329
Rizzi L., Held E. V., Bertelli G., Saviane I., 2003, ApJ, 589, L85

Romano D., Starkenburg E. 2013, MNRAS, 434, 471
Salpeter E. E., 1955, ApJ, 121, 161
Salvadori S., Ferrara A., 2009, MNRAS, 395, L6
Salvadori S., Ferrara A., 2012, MNRAS, 421, L29
Sand D. J., Olszewski E. W., Willman B., et al., 2009, ApJ, 704, 898
Shapley H., 1938, Harvard College Observatory Bulletin, 908, 1
Schmidt, 1959, ApJ, 129, 243
Shetrone M., Venn K. A., Tolstoy E., et al., 2003, ApJ, 125, 684
Siegel M. H., 2006, ApJ, 649, L83
Simon J. D., Frebel A., McWilliam A., Kirby E. N., Thompson I. B., 2010, ApJ, 716, 446
Starkenburg E., Hill V., Tolstoy E., et al., 2010, A&A, 513, A34
Starkenburg E., Hill V., Tolstoy E., et al., 2013, A&A, 549, A88
Tafelmeyer M., Jablonka P., Hill V., et al., 2010, A&A, 524, A58
Tolstoy E., Venn K. A., Shetrone M., et al., 2003, AJ, 125, 707
Tolstoy E., Hill V., Tosi M., 2009, ARA&A, 47, 371
van den Hoek L. B., Groenewegen M. A. T., 1997, A&AS, 123, 305
Vargas L. C., Geha M., Kirby E. N., Simon J. D., 2013, ApJ, 767, 134
Venn K. A., Shetrone M. D., Irwin M. J., et al., 2012, ApJ, 751, 102
Walker M. G., Mateo M., Olszewski E. W., et al., 2009, ApJ, 704, 1274
Wolf J., Martinez G. D., Bullock J. S., et al., 2010, MNRAS, 406, 1220
Woosley S. E., Weaver T. A., 1995, ApJS, 101, 181
Yin J., Matteucci F., Vladilo G., 2011, ApJ, 531, A136

This paper has been typeset from a TEX/ LATEX file prepared by the author.